Diurnal Circulations and Rainfall in Taiwan during SoWMEX/TiMREX (2008)

JAMES H. RUPPERT JR. AND RICHARD H. JOHNSON

Department of Atmospheric Science, Colorado State University, Fort Collins, Colorado

ANGELA K. ROWE

Department of Atmospheric Sciences, University of Washington, Seattle, Washington

(Manuscript received 4 October 2012, in final form 22 May 2013)

ABSTRACT

The diurnal cycle of the local circulation, rainfall, and heat and moisture budgets is investigated in Taiwan's heavy rain (mei-yu) season using data from the 2008 Southwest Monsoon Experiment/Terrain-influenced Monsoon Rainfall Experiment (SoWMEX/TiMREX). Comparisons are made between an undisturbed (UNDIST; 22–29 May) and disturbed period (DIST; 31 May–4 June). Many aspects of the diurnal evolution in surface flows and rainfall were similar during both periods. At night and during early morning hours, the low-level southwesterly flow was deflected around Taiwan's main topographic barrier, the Central Mountain Range (CMR), with rainfall focused near areas of enhanced offshore confluence created by downslope and land-breeze flows. During the day, the flow switched to onshore and upslope, rainfall shifted inland, and deep convection developed along the coastal plains and windward slopes. Atmospheric budget analysis indicates a day-to-evening transition of convective structure from shallow to deep to stratiform. Evaporation associated with the evening/nighttime stratiform precipitation likely assisted the nocturnal katabatic flow.

Though the flow impinging on Taiwan was blocked during both periods, a very moist troposphere and strengthened low-level oncoming flow during DIST resulted in more widespread and intense rainfall that was shifted to higher elevations, which resembled a more weakly blocked regime. Correspondingly, storm cores were tilted upslope during DIST, in contrast to the more erect storms characteristic of UNDIST. There were much more lofted precipitation-sized ice hydrometeors within storms during DIST, the upslope advection of which led to extensive stratiform rain regions overlying the CMR peaks, and the observed upslope shift in rainfall.

1. Introduction

A strong diurnal pulsation of rainfall is connected to coastal regions and areas of sloped topography in the tropics and subtropics, which are attended by prominent land–sea-breeze (LSB) and mountain–valley (MV) circulations. In the mountainous subtropical island of Taiwan, rainfall is controlled throughout the year by such circulations, which cause a pronounced diurnal oscillation in island-averaged low-level divergence (Johnson and Bresch 1991; Chen et al. 1999; Kishtawal and Krishnamurti 2001; Kerns et al. 2010; Lin et al. 2011). Great complexity is added to this system in the presence of monsoon flow, which interacts with Taiwan's main topographic barrier, the Central Mountain Range (CMR), to generate enhanced upstream convergence, barrier jets, offshore rainbands, and lee vortices (Sun and Chern 1993; Li and Chen 1998; Yeh and Chen 2002; Chen et al. 2004; Alpers et al. 2007; Yu and Lin 2008; Yu and Hsieh 2009). The manner in which such features interact with the diurnal cycle needs further investigation, as these two major aspects of Taiwan's meteorology have been studied quite separately to date. Improved understanding of the diurnal cycle of rainfall and its relationships with flow blocking was a core focus of the Southwest Monsoon Experiment/Terrain-influenced Monsoon Rainfall Experiment (SoWMEX/TiMREX; Jou et al. 2011), which was conducted during the 2008 heavy rain season in Taiwan (the mei-yu or ''plum rain'' season).

The mei-yu season in Taiwan covers the mid-May–mid-June period in which the stable northeasterly winter monsoon transitions to the convectively unstable

Corresponding author address: James H. Ruppert Jr., Dept. of Atmospheric Science, Colorado State University, 1371 Campus Delivery, Fort Collins, CO 80523.
E-mail: ruppert@atmos.colostate.edu

DOI: 10.1175/MWR-D-12-00301.1

southwesterly summer monsoon (Chen 1983, 1993; Ding and Chan 2005). During this season, a pronounced zone of low-level convergence and cyclonic shear will periodically develop where these flows meet (the mei-yu front), in connection with a strengthened southwesterly low-level jet, amplified upper-level flow pattern, and deepened East Asian monsoon trough (Chen 1983; Chen 1993; Chen et al. 2008). During such *disturbed conditions*, this subtropical mei-yu frontal system, which typically forms north of Taiwan, can shift southward into the Taiwan area and provide an effective triggering mechanism for copious rainfall through mesoscale convective systems (MCSs) that spawn and propagate eastward along its ~zonally oriented strip of barotropic vorticity (Chen 1983; Chen et al. 2008; Lai et al. 2011). Lai et al. (2011) documented a case from SoWMEX/TiMREX in which an MCS propagated offshore from southern China and organized into an intense mesoscale convective vortex (MCV), aided by stretching from deep convection along the mei-yu frontal vorticity line. Vigorous convection was favored downshear (east) of the MCV where northward advection of unstable low-level air was enhanced, which caused heavy rainfall along the mei-yu front and inland flooding as it propagated eastward across southern Taiwan. Shallow, rain-generated coastal boundaries unrelated to the mei-yu front can also be important for heavy rainfall during the mei-yu season (Davis and Lee 2012; Xu et al. 2012). While these boundaries typically exhibit virtual temperature contrasts of only 2°–3°C (cooler over land), they enhance nearshore and offshore convergence enough to invigorate free convection in the moist impinging southwesterly flow (Davis and Lee 2012; Xu et al. 2012).

Johnson and Bresch (1991) describe the diurnal cycle characteristic of mei-yu *undisturbed periods*; periods when the mei-yu front is either not present or is situated north of Taiwan, rainfall is reduced, and relatively uniform southwesterly flow impinges on Taiwan. They used observations from the 1987 Taiwan Area Mesoscale Experiment (TAMEX; Kuo and Chen 1990), and found that daytime sea breezes and anabatic flows strengthened in the late morning and early afternoon as deep convection increased along the coastal plains and western foothills of the CMR. Convection transitioned to stratiform rainfall by evening as evaporation-enhanced katabatic flows and land breezes developed. Finally, rainfall was maximized offshore during the overnight and early morning hours. Subsequent studies have employed satellite data as well as the dense rain gauge network in Taiwan to corroborate these findings and extend the analysis to other seasons (Chen et al. 1999; Kishtawal and Krishnamurti 2001; Kerns et al. 2010; Lin et al. 2011). These and other studies have primarily focused on undisturbed periods or seasonal means. It is important to assess the role and character of the diurnal cycle in more disturbed environments when conditions are more conducive for heavy rainfall, such as when the subtropical mei-yu front develops and shifts southward over Taiwan.

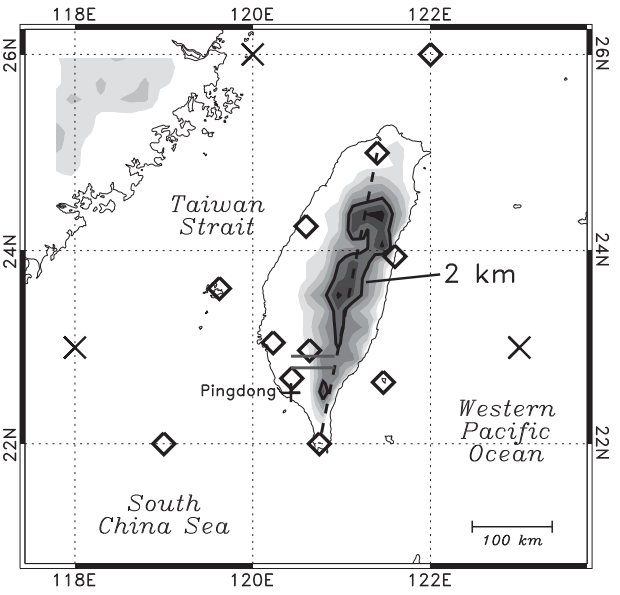

FIG. 1. Topography is gray shaded every 400 m. The 2-km level is contoured. Polygons denote 11 of the 13 rawinsonde stations constituting the SoWMEX/TiMREX enhanced sounding network. Sites not shown are Dongsha Island, located to the southwest (shown in Fig. 8) and Laoag, Philippines, located south of Taiwan. The plus sign denotes the S-Pol radar station, situated in coastal Pingdong. The crisscrosses (×s) denote three surrounding GFS data points incorporated in INTERP. The dashed line represents the dividing line for an area average over western Taiwan (see the appendix). The two solid lines north of Pingdong denote the transects for two west–east-oriented radar cross sections discussed later.

A major factor in the distribution and intensity of rainfall in Taiwan relates to the effects of topography. Figure 1 provides a topographic map of Taiwan showing the coastal plains in the west and the steep slopes of the CMR. Note that the CMR slopes extend down nearly to the eastern coastline, resulting in an east–west asymmetry in the distribution of lowlands surrounding the CMR. From theory, the Burger number B can be used to diagnose the ''hydrodynamic steepness'' of the mountain barrier, where $B = HN_m/fL$, H is the ridge height, N_m is the subsaturated moist Brunt–Väisälä frequency, f is the Coriolis parameter, and L is flow-parallel mountain half-width. When $B \ll 1$, the slope is mild and the flow remains in quasigeostrophic balance, and when $B \gg 1$, the slope is significant and ageostrophic flows divert around the barrier (Baines 1987; Pierrehumbert

and Wyman 1985; Smolarkiewicz et al. 1988; Overland and Bond 1995). Using approximations for Taiwan [$H \sim 2\,\text{km}$, $L \sim 50\,\text{km}$, $N_m \sim 10^{-2}\,\text{s}^{-1}$, and $f \sim 10^{-4}\,\text{s}^{-1}$; Li and Chen (1998)], $B = 4$, suggesting that the CMR is a hydrodynamically steep barrier that will block the flow. For any characteristic wind speed $U \leq 20\,\text{m}\,\text{s}^{-1}$, the Froude number $\text{Fr} = U/N_m H$ is subunity (using the approximations above), suggesting that the kinetic energy of the flow is small relative to the potential energy required to surmount the barrier; hence, the flow is diverted (Smolarkiewicz et al. 1988). While utility of a saturated Brunt–Väisälä frequency is apt in saturated conditions (e.g., Durran and Klemp 1982), saturation is limited to the scale of individual cloud systems when the prevailing upstream flow is subsaturated, as it was during SoWMEX/TiMREX; therefore, Fr as defined above is appropriate for diagnosing the predominate flow characteristics around Taiwan (Baines 1987; Smolarkiewicz et al. 1988; Carbone et al. 1995; Li and Chen 1998; Chen and Lin 2005; Hughes et al. 2009; Miglietta and Rotunno 2009).

Blocked flows around Taiwan result in areas of enhanced low-level convergence and rainfall surrounding the island; for example, quasi-stationary convective rainbands frequently appear offshore of southeastern Taiwan all year round in connection with flow blocking (Yu and Jou 2005; Yu and Hsieh 2009; Alpers et al. 2010). The pre-mei-yu-frontal heavy rainfall events in northwestern Taiwan offer another example of orographic rainfall enhancement (Li and Chen 1998; Yeh and Chen 2002; Wang et al. 2005). The Big Island of Hawaii provides a related example in which diurnal and orographic processes interact to produce a prominent arch-shaped rainband upwind of the island (Smolarkiewicz et al. 1988; Carbone et al. 1995). Initially, evaporative cooling from diurnal rainfall in the elevated terrain generates a nocturnal katabatic, offshore flow. The rainband forms offshore where this flow converges with the impinging stable trade wind. Finally, the rainband moves onshore as daytime heating drives a reversal to onshore, upslope flow. In addition to the general enhancement of rainfall by orography, rainfall distribution can be complicated by the flow–microphysical interactions that occur when widespread deep convection is present (Jiang 2003; Chen and Lin 2005; Miglietta and Rotunno 2009; Murphy and Businger 2011).

In the present study, the SoWMEX/TiMREX enhanced sounding network is employed to describe the diurnal cycle of mesoscale diurnal circulations and heat and moisture budgets (i.e., latent heating) over Taiwan, with comparison between undisturbed and disturbed conditions. Johnson and Bresch (1991) is the only prior study to do a similar examination, though the sounding network they employed (TAMEX) had marginal spatial coverage and diurnal variability during disturbed periods was not discussed. New estimates of the vertical and horizontal distributions of diabatic heating will provide a basis for validation and comparison with numerical simulations of the diurnal cycle over Taiwan.

2. Datasets and methodology

a. Gridded dataset

Previous studies have successfully employed objective interpolation procedures to sounding datasets from a number of tropical and monsoon field campaigns [e.g., the Tropical Ocean and Global Atmosphere Coupled Ocean–Atmosphere Response Experiment (TOGA COARE), the South China Sea Monsoon Experiment (SCSMEX), and North American Monsoon Experiment (NAME)], and obtained reliable results confirmed by the analysis of independent datasets (Lin and Johnson 1996; Johnson and Ciesielski 2002; Ciesielski et al. 2003; Johnson et al. 2010). A similar approach is followed in this study, which allows dynamical relationships to emerge from observations with minimized influence from model information.

A gridded analysis (denoted INTERP) is generated on a 0.25° mesh from 18°N, 112°E to 28°N, 124°E with 40 vertical levels (surface and 1000–50 hPa at 25-hPa increments) by running observations through the multiquadric interpolation scheme of Nuss and Titley (1994). The main sampling period of SoWMEX/TiMREX (special observing period; SOP) spanned 15 May–26 June 2008, during which time a dense network of rawinsondes, radars, wind profilers, and surface stations was deployed in and around Taiwan (Jou et al. 2011). The SoWMEX/TiMREX sounding network was composed of 13 sites, including land stations in and bordering Taiwan and stations in the northern South China Sea (SCS) and Taiwan Straight (Fig. 1). Six-hourly soundings were taken at most sites during the SOP, with 3-hourly soundings during a roughly weeklong enhanced observing period (EOP) during late May–early June. During the EOP the mei-yu front amplified and shifted southward into the northern SCS (Lai et al. 2011; Davis and Lee 2012). Sixteen dropsonde missions (yielding 190 soundings) were also carried out during this EOP and a later active period. Ciesielski et al. (2010) describe the extensive SoWMEX/TiMREX sounding dataset and quality control procedures, which resulted in substantial improvements in the humidity field (removal of dry biases).

The observations employed in INTERP are listed in Table 1. Operational soundings from China are included to supplement the SoWMEX/TiMREX sounding dataset

TABLE 1. Observations used for the SoWMEX/TiMREX interpolated analysis (INTERP).

Observation type	Source	Approx quantity per analysis	Daily frequency in INTERP (during the EOP)
Standard upper air (up- and dropsonde)	SoWMEX/TiMREX and operational datasets (China and Taiwan)	10 000 (32 sondes)	4 (8)
Sea surface wind	QuikSCAT	300–1150	2 (2)
Standard surface	Taiwan's CWB and Meteorological Assimilation Data Ingest System (MADIS)	200	4 (8)
Vertical profiler wind	CWB (operational)	60	4 (8)

away from Taiwan (yielding a total of 32 sounding sites). Quick Scatterometer (QuikSCAT) sea surface wind data were filtered to 0.25° spacing prior to the interpolation, with all rain- and land-contaminated data excluded. Similar to previous studies employing this technique (e.g., Johnson and Ciesielski 2002), inclusion of data from operational 0.5° National Centers for Environmental Prediction (NCEP) Global Forecast System (GFS) analyses at several points outside of the main sounding network (Fig. 1) was necessary to minimize the effects of extrapolation into data-sparse regions (particularly east of Taiwan, where flow blocking can substantially modify the far flow fields). The impacts were primarily on mean magnitudes, while the day-to-day and diurnal variabilities were primarily reflecting observations. This is discussed further in the appendix. Due to sampling errors in sounding observations (Mapes et al. 2003), 3-day running means are applied to SOP time series based on INTERP fields to increase the statistical significance. Additional details of the multiquadric procedure can be found in Ciesielski et al. (2003).

b. *Independent datasets*

To diagnose characteristics of afternoon thunderstorms during focal periods of the study, two cross sections are generated using data from the National Center for Atmospheric Research (NCAR) S-band dual-polarization Doppler radar (S-Pol) that was deployed in southwestern coastal Taiwan during SoWMEX/TiMREX (22.53°N, 120.43°E; Fig. 1). Full-volume 360° surveillance scans allowed for rain mapping to a maximum range of 150 km along the western slopes of the CMR, enabling comparisons and coordination with the neighboring Pingdong sounding station. Quality control of the S-Pol dataset followed the methods of Lang et al. (2007). The corrected suite of polarimetric variables (cf. Rowe et al. 2011, 2012) was gridded to Cartesian coordinates at 1-km horizontal and 0.5-km vertical grid spacing using the program REORDER (Mohr et al. 1986). A hydrometeor identification (HID) algorithm was applied to infer the dominant hydrometeor types at each grid point, including drizzle (DZ), rain (RA), dry snow (DS), wet snow (WS), vertical ice (IC), low-density graupel (LG), high-density graupel (HG), and hail (HA). This HID algorithm, which employed the gridded polarimetric variables and temperature profiles from the Pingdong sounding station (Fig. 1), is based on the fuzzy-logic methodology of Liu and Chandrasekar (2000), and is described in detail by Tessendorf et al. (2005).

Rainfall from the Quantitative Precipitation Estimation and Segregation Using Multiple Sensors (QPESUMS) dataset is employed, which combines information from Taiwan's network of operational radars (i.e., not S-Pol) and rain gauges operated by the Central Weather Bureau of Taiwan, and is available hourly at 0.0125° spacing over and immediately surrounding Taiwan. Taiwan's operational rain gauge network is quite dense (Chen et al. 1999; Kishtawal and Krishnamurti 2001; Kerns et al. 2010), thus providing a good check on radar-derived rainfall. A concern in the QPESUMS dataset is offshore negative rainfall biases related to radar beam blockage, particularly near southeastern Taiwan (Chang et al. 2009). As will be shown, the resulting errors in southeastern Taiwan are often obvious, particularly during rainy periods; the discounting of data where this occurs is therefore straightforward. The Tropical Rainfall Measuring Mission (TRMM; Kummerow et al. 2000) 3B42v6 rainfall dataset (Huffman et al. 2007) is also employed, which is available every 3 h at 0.25° spacing. The TRMM 3B42v6 product (simply denoted TRMM hereafter) includes infrared (IR) brightness temperature data to fill in time gaps, leading to erroneous assignments of rainfall in areas of large nonraining high clouds (Liu et al. 2007). This TRMM dataset is useful for the study, however, in that it provides valuable information away from Taiwan where neither the rain gauge network nor radars do so.

c. *Diagnostic quantities*

Following Yanai et al. (1973), vertical profiles of the *apparent heat source* Q_1 and *apparent moisture sink* Q_2 are calculated, which enable diagnosis of precipitating systems from large-scale sounding measurements. These terms are defined as follows:

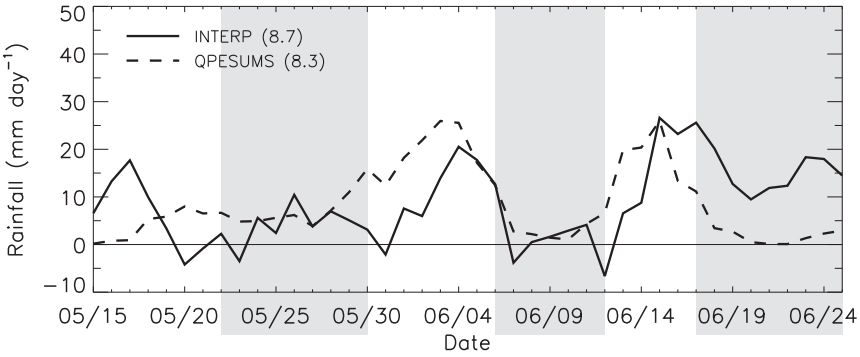

FIG. 2. SoWMEX/TiMREX SOP time series of rainfall (mm day^{-1}) averaged over Taiwan from INTERP and the QPESUMS dataset. Rainfall is diagnosed for INTERP from the moisture budget, as described in section 2c. The numbers in parentheses are SOP means. Gray shading denotes undisturbed periods. Rainfall estimates were smoothed using a 3-day running mean.

$$Q_1 \equiv \frac{\partial \overline{s}}{\partial t} + \overline{\mathbf{v}} \cdot \nabla \overline{s} + \overline{\omega} \frac{\partial \overline{s}}{\partial p} = Q_R + L(\overline{c} - \overline{e}) - \frac{\partial \overline{\omega' s'}}{\partial p}, \quad (1)$$

$$Q_2 \equiv -L\left(\frac{\partial \overline{q}}{\partial t} + \overline{\mathbf{v}} \cdot \nabla \overline{q} + \overline{\omega} \frac{\partial \overline{q}}{\partial p}\right) = L(\overline{c} - \overline{e}) + L \frac{\partial \overline{\omega' q'}}{\partial p}, \quad (2)$$

where $s = c_p T + gz$ is dry static energy, $\mathbf{v}$ is horizontal wind, ω is vertical pressure velocity, Q_R is radiative heating, L is latent heat of vaporization, c is condensation rate, e is evaporation rate, q is water vapor mixing ratio, c_p is specific heat of dry air, T is temperature, g is gravitational acceleration, z is height, the overbar denotes an area average, and the prime represents the eddy component. The Lagrangian tendencies of heat s and moisture q [i.e., the left-hand sides of (1) and (2)] are directly calculated from INTERP. Then, Q_1 and Q_2 are divided by c_p to express them in temperature tendencies. Divergence δ is vertically mass balanced by assuming adiabatic flow at the tropopause and using a constant divergence correction (O'Brien 1970), and δ is vertically integrated to diagnose ω. The lower boundary for ω is determined by calculating the slope flow (Luo and Yanai 1983).

Estimated rainfall rate is calculated for INTERP by vertically integrating Q_2 and adding surface latent heat flux LH to close the moisture budget (Yanai et al. 1973). LH estimates were obtained from the European Centre for Medium-Range Weather Forecasts' Year of Tropical Convection (YOTC) analyses (Waliser et al. 2012). Inaccuracies in budget-derived rainfall can result from errors in Q_2 (the moisture and/or kinematic fields), poor LH estimates from YOTC, and the neglect of water vapor storage in clouds (McNab and Betts 1978; Johnson 1980).

3. SoWMEX/TiMREX overview

As demonstrated by a time series of daily mean rainfall averaged over Taiwan (Fig. 2), rainfall varied substantially through the SOP, with approximately a week separating two rainy (disturbed) periods (discussed below). INTERP exhibits wet biases early and late in the SOP relative to QPESUMS (i.e., ending ~18 May and beginning ~17 June, respectively). During these periods, the SoWMEX/TiMREX sounding network was not in full operation (Ciesielski et al. 2010), and hence there was likely poor sampling of the complex, blocked flow around Taiwan. However, apart from the 1–2-day rainfall delay relative to QPESUMS evident during the two disturbed periods, INTERP properly captures the rainfall magnitudes and general pattern of rainfall evolution.

Figure 3 provides SOP time–pressure sections of daily mean fields averaged over Taiwan from INTERP, including zonal and meridional flows u and v and relative humidity (RH). Onset of the low-level southwesterly flow occurred around 22 May, which coincided with a period of deep moisture following passage of a 200-hPa trough (on ~19 May). Two subsequent moist periods can be identified, with progressively drier periods separating them. Figure 4 provides SOP time–pressure sections of δ, ω, Q_1, and Q_2. The three dry (undisturbed) periods can be identified in Figs. 2–4 by reduced rainfall and tropospheric RH, abated tropospheric flow, and predominant subsidence (mid- to late-May, 6–12 June, and 17–25 June). The third undisturbed period is an exception, which exhibits weak rising motion, heating, and drying in Fig. 4. With such dry conditions aloft (Fig. 3) and negligible rainfall in QPESUMS (Fig. 2), however, it can be assumed that the rising motion,

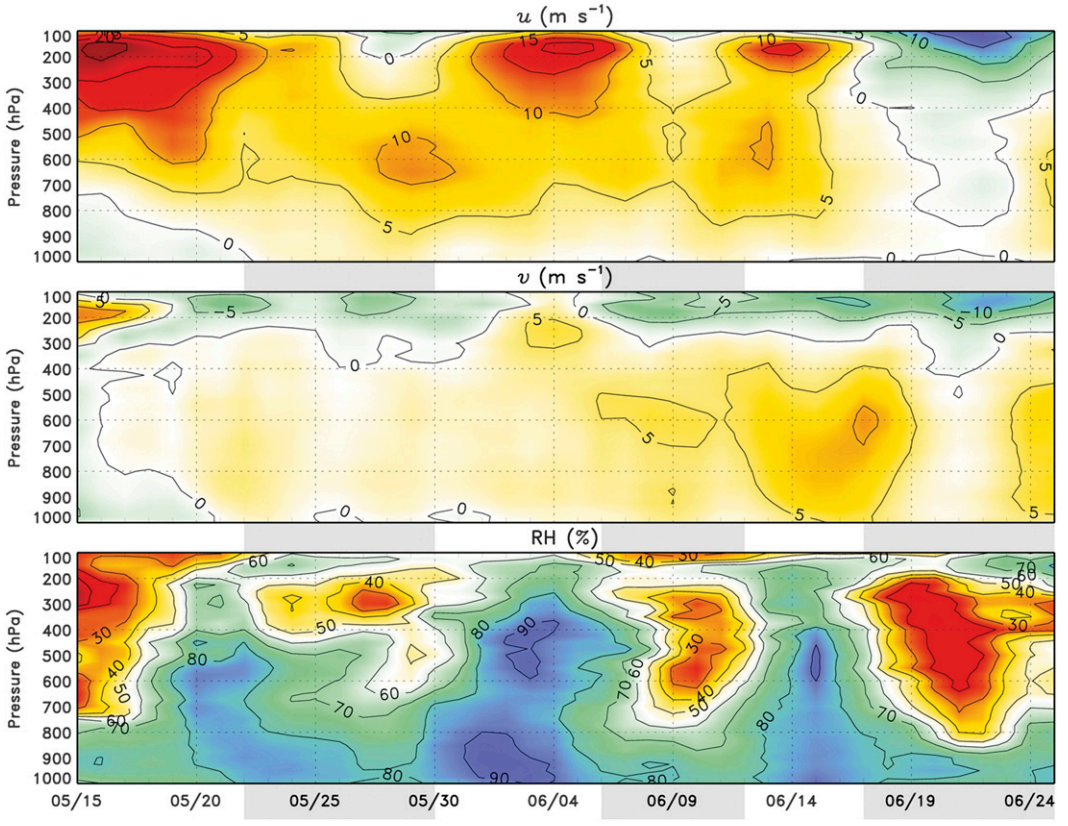

FIG. 3. SOP time–pressure sections averaged over Taiwan from INTERP (dates along the abscissa), including (top) daily mean zonal wind u ($\mathrm{m\,s^{-1}}$), (middle) meridional wind v ($\mathrm{m\,s^{-1}}$), and (bottom) relative humidity RH (%), with respect to ice where temperature $T < 0$°C. Fields were smoothed using a 3-day running mean.

heating, and drying are likely erroneous. This demonstrates that reductions in sounding frequency and coverage during this period degraded the ability of the SoWMEX/TiMREX sounding network to accurately capture the environment. The third and driest undisturbed period coincides with a switch to 200-hPa northeasterly flow, reflecting a northward shift of the 200-hPa Asian anticyclone.

The early and mid-June disturbed periods were characterized by deep moisture, strengthened tropospheric flow, and deep rising motion, heating, and drying (Figs. 3 and 4). Low-level cooling (negative Q_1) during the early June disturbed period indicates more stratiform rainfall compared with that in mid-June, which was apparently more convective in nature. During the roughly weeklong period preceding the early June disturbed period, strengthened westerly momentum descended from the upper troposphere (Fig. 3). Tropospheric moistening then commenced (~29 May), suggesting the establishment of the southwesterly moisture stream (Ding and Chan 2005). Heavy rainfall developed in Taiwan around 2 June (Figs. 2 and 4), by which time the mei-yu front had developed and shifted southward into the northern SCS, where it remained through 5 June. Passage of a 200-hPa trough (with $u > 20\,\mathrm{m\,s^{-1}}$) can be noted during this disturbed period (Fig. 3). Chen (1993) found that mei-yu fronts during TAMEX were associated with an amplifying wave pattern in which the Asian anticyclone shifted northward over the Tibetan Plateau and the midlatitude westerly jet shifted southward to the Taiwan area. As discussed by Lai et al. (2011), an MCV spun up along the mei-yu front during this active period and impacted southern Taiwan on 5 June. The mid-June disturbed period was unrelated to a mei-yu front. MCSs first propagated across southern Taiwan, leaving a residual cold pool (14–15 June). A quasi-stationary MCS then developed offshore, where moist southwesterly flow (Fig. 3) overrode this cold pool (15–16 June). Davis and Lee (2012) and Xu et al. (2012) discuss this case in detail.

Figure 5 provides time series of 3-hourly and daily mean measurements of sensible heat (SH), T, LH, and q from the National Taiwan University (NTU)

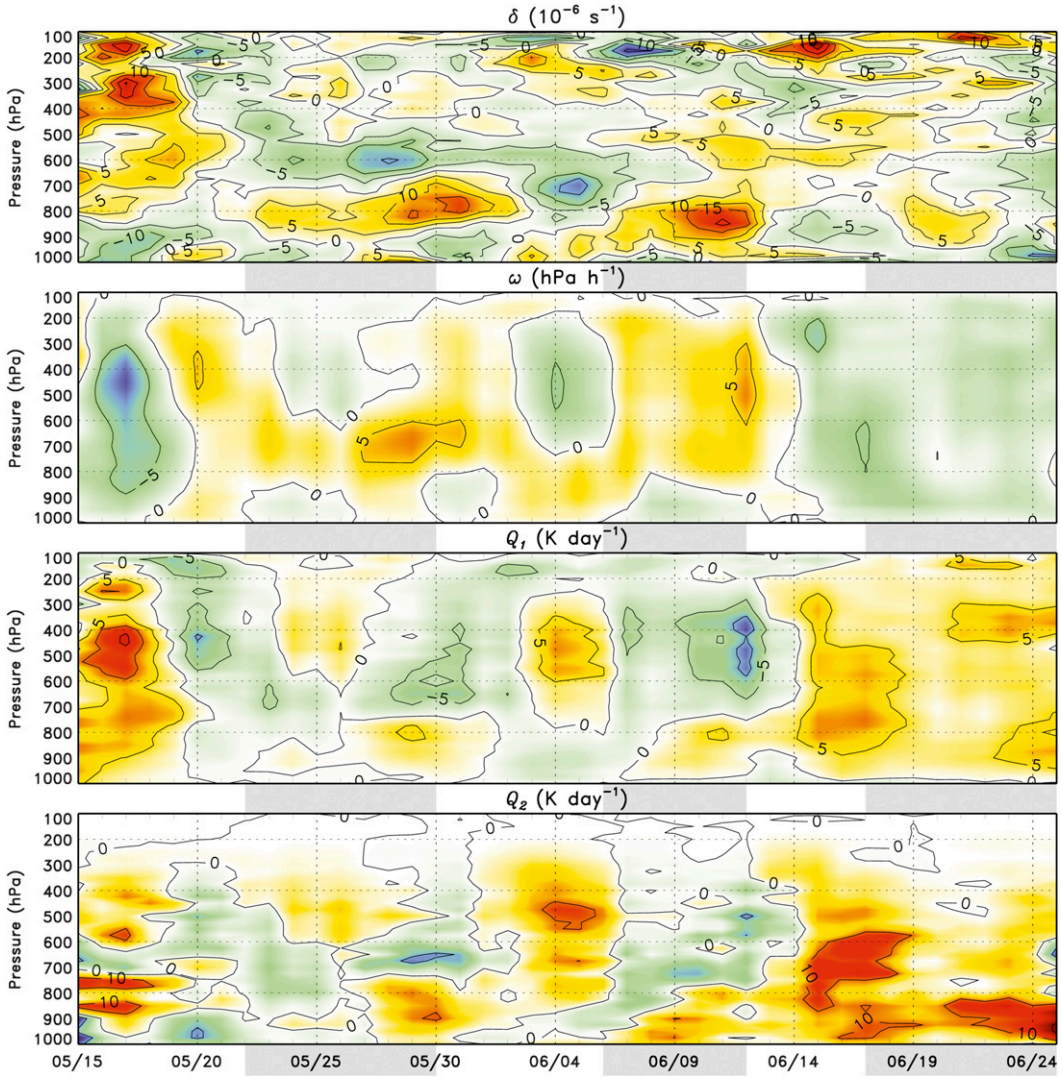

FIG. 4. As in Fig. 3, but with (top) divergence δ (10^{-6} s^{-1}), (second from top) vertical pressure velocity ω (hPa h^{-1}), (third from top) apparent heat source Q_1 (K day^{-1}), and (bottom) apparent moisture sink Q_2 (K day^{-1}).

experimental forest flux site at Pingdong (Fig. 1; note that data are only available through mid-June). The magnitude of the diurnal cycle in SH evolves in concert with daily mean SH; for example, note decreases in both in late May related to increasing cloud cover with the southward-advancing mei-yu front (Davis and Lee 2012). A similar evolutionary pattern can be noted in T. Diurnal variability in T and SH persists through the early June disturbed period, though it is reduced relative to the undisturbed periods. There is a steady increase in daily mean and 3-hourly LH with the progression of the mei-yu season, reflecting moistening soil and vegetation green up. Daily mean q increases similarly, with notable jumps near monsoon onset and the start of the early-June disturbed period.

Provided in Fig. 6 are hourly T' (Taiwan-averaged T with the SOP mean removed) and slope flow U_{SLOPE}, defined as the surface flow component parallel to the surface height gradient, averaged over Taiwan (positive values denote upslope).[1] Values of T' and U_{SLOPE} are calculated using observations from 55 quality-controlled surface stations in Taiwan, following multiquadric interpolation (Nuss and Titley 1994) onto a 0.25° mesh.

[1] As described in section 2, U_{SLOPE} is directly proportional to surface ω.

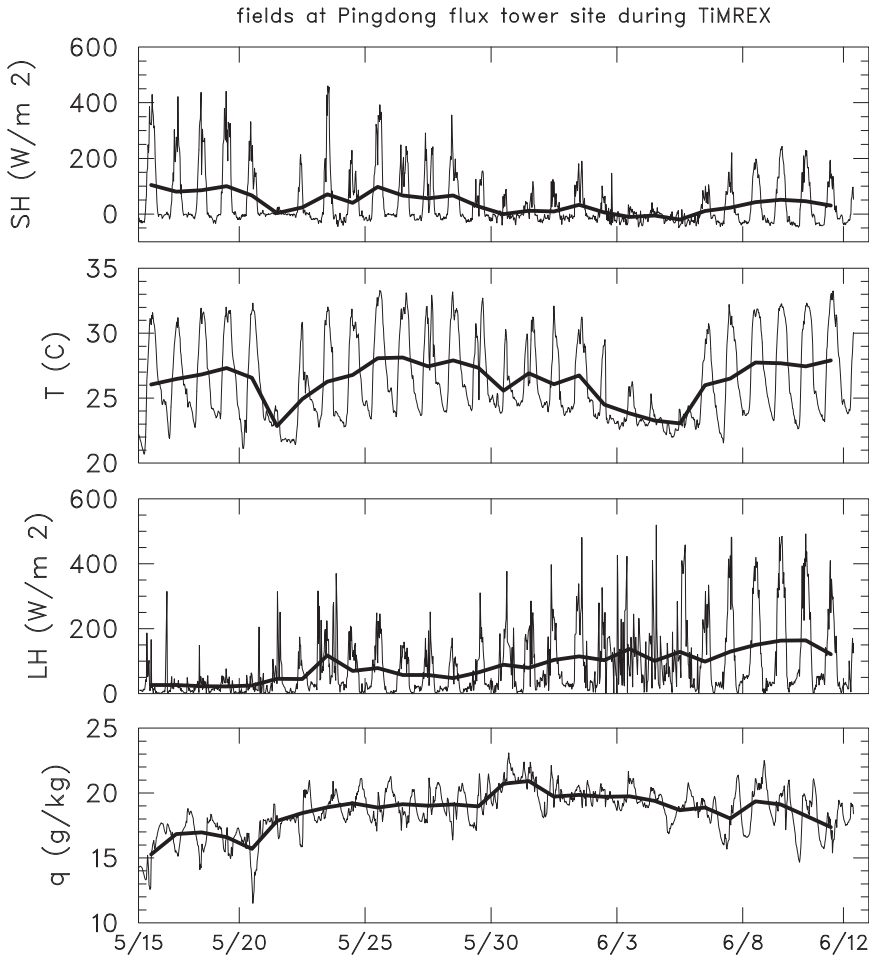

FIG. 5. Time series of flux tower measurements from Pingdong (Fig. 1), with (top) SH ($W m^{-2}$), (second from top) T (°C), (third from top) LH ($W m^{-2}$), and (bottom) water vapor mixing ratio q ($g kg^{-1}$). Data are shown in both 3-hourly (thin) and daily mean (thick) forms. Abscissa tick marks indicate local midnight. The time series ends in mid-June, after which point data are unavailable. (Data provided courtesy of Dr. P.-H. Lin.)

Taiwan-averaged QPESUMS rainfall is also provided in Fig. 6 in hourly and 3-day running mean forms.

Diurnal variation of U_{SLOPE} reflects the combined LSB and MV circulations (Fig. 6). Morning and afternoon perturbations to the regular diurnal cycle are likely related to LSB fronts and convective outflows. Both T' and U_{SLOPE} reach maximum [~1300 local time (LT)] and minimum (~0300 LT) near the same time each day. Rainfall maximizes between 1500 and 1800 LT on most days throughout the SOP, demonstrating the strong coupling of rainfall to the diurnal cycle. There is a several-hour offset between maximum T' and U_{SLOPE} and peak rainfall on many days (e.g., 26 May), as noted in other studies (Johnson and Bresch 1991; Kerns et al. 2010). Similar to T and SH from the Pingdong flux tower (Fig. 5), rainfall activity (i.e., smoothed rainfall) and the magnitude of the diurnal cycle in T' and U_{SLOPE} are inversely related. However, while the diurnal cycles in T' and U_{SLOPE} are greatly reduced during the two June disturbed periods, afternoon rainfall peaks are still observed on most days. Furthermore, the early June disturbed period exhibits a regular, albeit reduced, diurnal cycle in T' and U_{SLOPE}.

4. Analysis of the diurnal cycle

Next, compositing is employed to compare the diurnal cycles of two periods of the SOP (indicated in Fig. 6): an undisturbed period (UNDIST) spanning 22–29 May (8 days) and a disturbed period (DIST) spanning 31 May–4 June (5 days). The two June undisturbed periods were excluded from UNDIST composites because very dry conditions aloft resulted in suppressed rainfall (Figs. 3 and 6). The mid-June disturbed period was

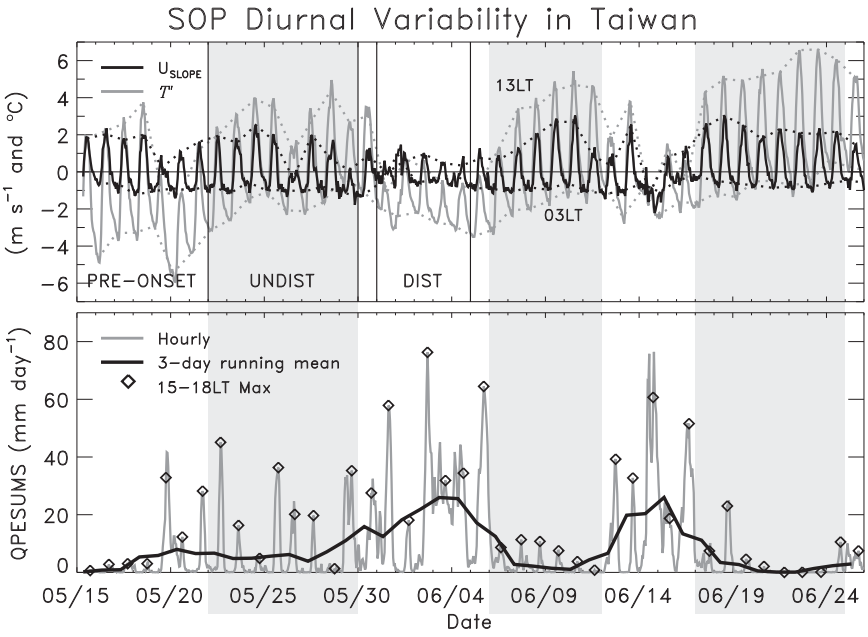

FIG. 6. (top) Hourly time series of U_{SLOPE} (positive for upslope; m s^{-1}) and T' (°C). Both are averaged over Taiwan and generated from surface stations. The 1300 and 0300 LT values are traced out with dotted lines. (bottom) Hourly and smoothed (using a 3-day running mean) QPESUMS rainfall (mm day^{-1}) averaged over Taiwan. Polygons denote the afternoon (1500–1800 LT) maximum rainfall each day. Abscissa tick marks indicate local midnight. Gray shading denotes undisturbed periods. Black vertical lines denote the bounds of the UNDIST (22–29 May) and DIST (31 May–4 Jun) periods for compositing.

excluded from DIST composites since it was characterized by substantial synoptic variability (Fig. 6; Davis and Lee 2012; Xu et al. 2012), offering poor persistence for a composite analysis. In addition, 5 June is excluded from DIST composites since much of the circulation and rainfall activity on that day was related to the propagation of an intense MCV across the island (Lai et al. 2011).

UNDIST is a characteristic period of monsoonal moist southwesterly flow in a subsidence-dominated, dry troposphere (Figs. 2 and 3), with a pronounced diurnal cycle in T, slope flows, and rainfall (Fig. 6). DIST is characteristically different from UNDIST in that there is much heavier rainfall (Fig. 2), strengthened southwesterly monsoon flow overriding a mei-yu front in the northern SCS, and deep moisture in connection with the upstream moistening by frontal lifting and associated convection (Fig. 3). Diurnal variability evidently persisted through DIST (Fig. 6). The goal herein is to address how the differing environmental characteristics between the two periods are manifested in the diurnal cycle of rainfall and circulations.

Compositing is performed by averaging variable time series for UNDIST and DIST as a function of time of day. Six-hourly composites are generated for UNDIST, and 3-hourly composites for DIST, since it coincided with the EOP. Figure 7 provides time series of diurnal composite rainfall from INTERP and QPESUMS for UNDIST and DIST. During UNDIST, QPESUMS rainfall ramps up slowly through the morning, with intensification around noon related to the onset of convection (Johnson and Bresch 1991; Kishtawal and Krishnamurti 2001; Kerns et al. 2010). With 6-hourly sampling, INTERP cannot properly resolve this intensification or the exact timing of the peak, though the general evolution and maximum value have merit.

Afternoon rainfall in QPESUMS is doubled during DIST (Fig. 7, bottom), with rainfall observed throughout the day. QPESUMS rainfall intensifies around noontime, similar to UNDIST, likely reflecting the onset of deep convection. The absence of nighttime and morning rainfall in INTERP seems dubious. Evidence suggests that the magnitudes of mean Q_1 and Q_2 in INTERP may have slight errors owing to difficulties in sampling the complex orographically enhanced gradients in temperature and moisture across the CMR (where there are little data; Fig. 1) and between Taiwan and the surrounding region. In particular, horizontal gradients in s and q along the coastal plain are not well represented owing to the lack of sounding data over the interior of Taiwan, such that

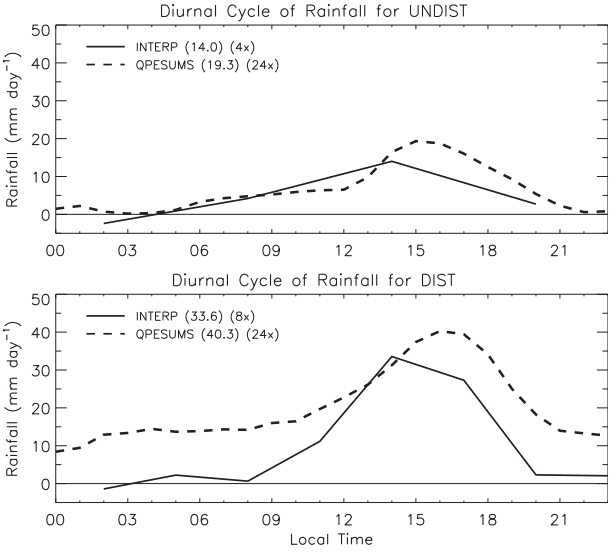

FIG. 7. Time series of diurnal composite rainfall (mm day^{-1}) averaged over Taiwan for (top) UNDIST and (bottom) DIST from INTERP and QPESUMS. First numbers in parentheses are maximum values and second are samples per day.

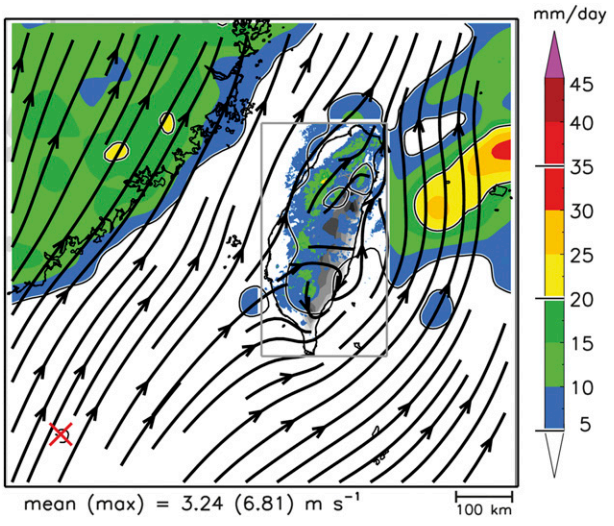

FIG. 8. UNDIST mean surface streamlines from INTERP (mean and maximum domain wind speed values provided at bottom) and rainfall (mm day^{-1}). QPESUMS rainfall is shaded (color scale at right), and TRMM rainfall is contoured at 5, 20, and 35 mm day^{-1} inside of the QPESUMS domain (gray rectangle) and shaded surrounding it. The red crisscross (×) marks the Dongsha Island sounding station. Terrain is gray shaded as in Fig. 1.

terrain-induced subsidence warming and drying are not offset by horizontal advection (M. Toy 2012, personal communication). However, INTERP properly captures the diurnal rainfall evolution. Three-hourly sampling during this period provides more detailed diurnal structure. Morning intensification of and peak rainfall occur slightly earlier than in QPESUMS (roughly one time step in INTERP). This bias may be related to water storage in developing clouds, which would be reflected as rainfall in the moisture budget (McNab and Betts 1978; Johnson 1980).

a. Undisturbed period (UNDIST): 22–29 May 2008

The flow is predominant southwesterly during UNDIST, according to a map of UNDIST mean surface streamlines and QPESUMS and TRMM rainfall (Fig. 8); however, there is an area of diffluence and confluence upstream and downstream of Taiwan, respectively, related to flow blocking by Taiwan (section 1). A mean upstream sounding for UNDIST from Dongsha Island (location indicated in Fig. 8; sounding not shown) indicates that Fr ~ 0.3 in the 700–950-hPa layer, with layer-mean flow $U \sim 8\,\mathrm{m\,s^{-1}}$; thus, the low-level ambient flow is blocked by Taiwan. Consistent with a blocked-flow regime, rainfall is maximized upstream of the terrain peaks (i.e., along the coastal plains and lower CMR slopes) and along and offshore of the northwestern coast (Hughes et al. 2009). There is very little rainfall southwest of Taiwan. With regard to the area of TRMM rainfall east of Taiwan, which is barely hinted at by QPESUMS, there are neither upper-air data nor other observations to verify its existence; hence, it will not be discussed in this study.

Figure 9 presents maps of UNDIST diurnal composite rainfall (3 hourly) and surface flow patterns (6 hourly). Diurnal surface flow anomalies (Fig. 9a) are generated by removing the UNDIST mean from the diurnal composites (Fig. 9b). The diurnal flow anomalies demonstrate a pronounced reversal over Taiwan's slopes and over the Taiwan Strait, which reflects the oscillating LSB and MV circulations (Fig. 6). The flows retaining the composite mean (Fig. 9b) demonstrate how this evolution manifests in the low-Fr ambient flow. From 0200 to 0800 LT, streamlines are diverted around Taiwan, with enhanced streamline confluence in the Taiwan Strait in connection with nocturnal downslope and offshore flows in Taiwan and China (Fig. 9a). At 0500 LT (near sunrise), coastal rainbands can be noted around the island, with a marked example near northwestern-coastal Taiwan (Fig. 9a). This pronounced rainband resembles the orographically enhanced convective rainbands often observed southeast of Taiwan (Yu and Jou 2005; Alpers et al. 2007; Yu and Lin 2008) and the arc-shaped rainband observed in the blocked trade wind flow upstream of the Big Island of Hawaii (Smolarkiewicz et al. 1988). From 0500 to 1100 LT, showers move onshore and increase in coverage over Taiwan as anomalous downslope and offshore flows weaken (Fig. 9a). By 1400 LT, there is pronounced anomalous onshore and upslope flow (Fig. 9a) and rainfall has increased in intensity and

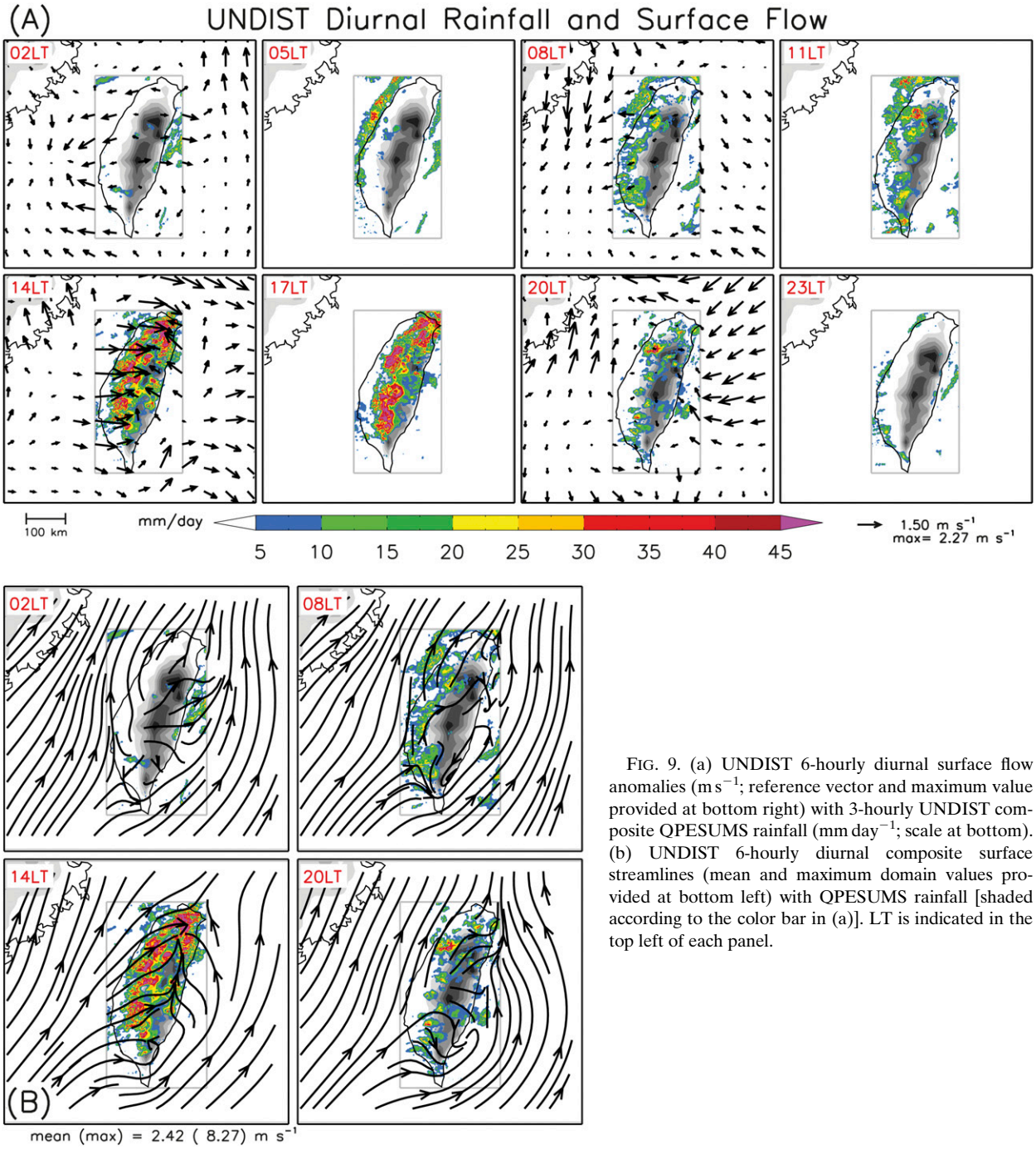

FIG. 9. (a) UNDIST 6-hourly diurnal surface flow anomalies ($m\,s^{-1}$; reference vector and maximum value provided at bottom right) with 3-hourly UNDIST composite QPESUMS rainfall ($mm\,day^{-1}$; scale at bottom). (b) UNDIST 6-hourly diurnal composite surface streamlines (mean and maximum domain values provided at bottom left) with QPESUMS rainfall [shaded according to the color bar in (a)]. LT is indicated in the top left of each panel.

coverage over the coastal plains and windward slopes, reflecting the development of deep convection (Kishtawal and Krishnamurti 2001). Whereas the southwesterly streamlines bow slightly around Taiwan during the morning and overnight, they are directed inland and traverse the CMR at 1400 LT (Fig. 9b). Rainfall coverage increases further by 1700 LT. By 2000 LT, the rainfall has substantially dissipated, and the flow has returned to downslope (Fig. 9b). Rainfall is organized in close alignment with the Taiwan coast at 2300 LT (Fig. 9a), suggesting the development of land-breeze fronts.

Area-averaged vertical profiles of δ, ω, Q_1, and Q_2 for UNDIST over Taiwan are shown in Fig. 10 as both period averages and diurnal composite time series. The lowest levels in these profiles (i.e., below 800 hPa) primarily reflect coastal data, since inland points are

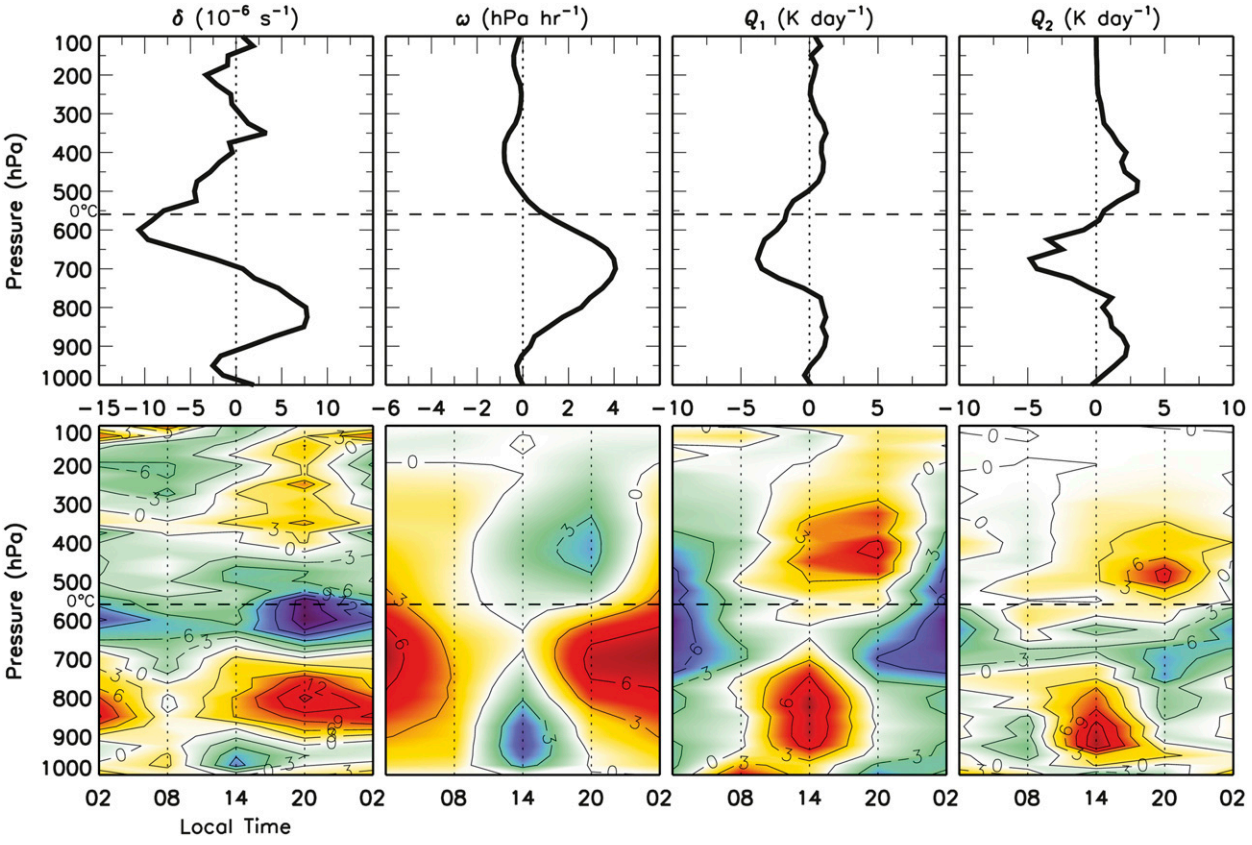

FIG. 10. UNDIST composite vertical profiles from INTERP averaged over Taiwan in (top) mean and (bottom) diurnal composite forms (6-hourly sampling). (From left to right) δ (10^{-6} s^{-1}), ω (hPa h^{-1}), Q_1 (K day^{-1}), and Q_2 (K day^{-1}). The 0°C level is dashed. Abscissas indicate (top) mean values and (bottom) LT. The 0200 LT values are repeated in diurnal profiles for continuity.

below ground. Also, since the CMR is displaced east of center in Taiwan (Fig. 1), characteristics of the western slopes dominate these averages. This spatial bias is discussed further in the appendix. In the mean there is pronounced low-level divergence and midlevel convergence, which is associated with subsidence from ~900 hPa to midlevels and weak rising motion aloft. Lower-tropospheric divergence and sinking motion are consistent with the upwind splitting of blocked, low-Fr flow, as discussed earlier. The vertical patterns in mean Q_1, and Q_2—warming and drying above cooling and moistening—suggest that stratiform rain is the predominant form of precipitation (Houze 1982; Johnson 1984). However, evidence suggests that the magnitudes of the mean Q_1 and Q_2 may have slight errors associated with unresolved horizontal gradients in temperature and moisture in and around Taiwan (see earlier discussion of this topic). In spite of these potential errors, the diurnal evolution depicted in Fig. 10 is sound and consistent with previous studies of diurnal rainfall in Taiwan (e.g., Johnson and Bresch 1991; Kishtawal and Krishnamurti 2001). For example, upper-level divergence coincides with rising motion, warming, and drying through most of the column around 1400 LT, demonstrating that afternoon precipitation is predominantly convective (Fig. 10, bottom panels). The timing of deep convection is consistent with the diurnal rainfall evolution during UNDIST based on both INTERP and independent observations (Figs. 7 and 9).

In the early morning (0200 LT), sinking motion and low-level divergence can be noted, and are associated with the land breeze and katabatic flow. By midmorning a shallow layer of convergence develops near the surface associated with the sea breeze and anabatic flow, which follows a low-level divergence maximum that ascends with time into the afternoon. This convergence–divergence pattern is consistent with the development of a shallow cumulus field in response to island heating. Similar results were found over the mountains of northwestern Mexico during the NAME (Johnson et al. 2010). Low-level heating (0800 LT) precedes low-level rising motion, presumably as a result of eddy heat flux convergence in the boundary layer after sunrise. Deep convection develops by 1400 LT, as indicated by

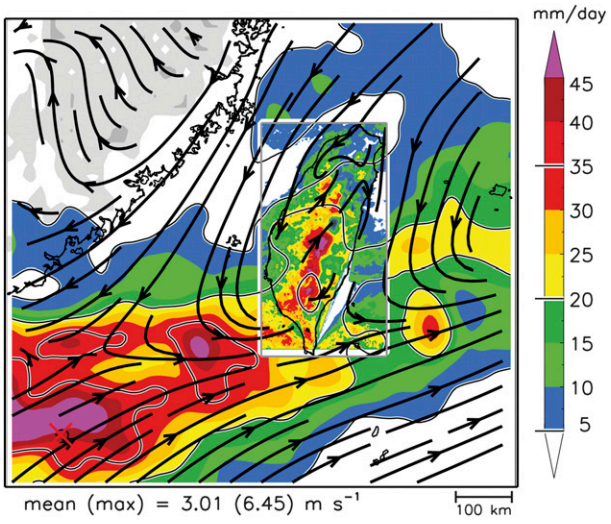

FIG. 11. As in Fig. 8, but for DIST.

divergence around 300 hPa and upper-level rising motion, heating, and drying. This coincides with the development of upslope flow and inland rainfall (Figs. 9 and 10). A pronounced stratiform rainfall pattern develops by afternoon (2000 LT), as indicated by strengthened upper-tropospheric divergence, convergence around the 0°C level, and lower- (upper-) tropospheric sinking (rising) motion (Johnson and Bresch 1991; Kishtawal and Krishnamurti 2001). In noting that this stratiform rain transition coincides with the development of downslope flows (Fig. 9b), a connection can be inferred between evening rainfall evaporation (i.e., lower-tropospheric cooling and moistening) and the onset of a nocturnal katabatic regime, similar to the Big Island of Hawaii (Carbone et al. 1995).

b. Disturbed period (DIST): 31 May–4 June 2008

A map of mean surface streamlines and rainfall for DIST (Fig. 11) clearly depicts the mei-yu front, which separates the southwesterly summer monsoon flow from the northeasterly flow to the north. There is a clear concentration of rainfall along and south of the frontal confluence line, which is largely associated with eastward-propagating frontal MCSs (Chen 1983; Lai et al. 2011; Davis and Lee 2012). Several southwesterly streamlines can be noted in Taiwan, reflecting the shallow nature of the mei-yu front (Chen 1983). Because of more widespread rainfall during DIST, the QPESUMS issue related to radar beam blockage offshore of southern Taiwan is clearly visible in Fig. 11.

In Taiwan, the rainfall is shifted higher along the windward slopes relative to UNDIST (Figs. 8 and 11). Based on a mean sounding for DIST from Dongsha Island (not shown), Fr $\sim$ 0.6 over 700–950 hPa, with $U \sim 14\,\mathrm{m\,s^{-1}}$ at that layer. The upslope shift in rainfall relative to UNDIST is consistent with larger U and Fr, which suggests reduced flow blocking [though Fr remains <1; Hughes et al. (2009)]. With a very moist troposphere (Fig. 3) and larger U and Fr, however, the atmosphere is conducive to more vigorous and/or widespread deep convection during this period. The importance of differing convective storm characteristics from UNDIST in more weakly blocked flow will be assessed in section 5.

Figure 12 provides maps of diurnal composite rainfall and surface flows (now 3 hourly) for DIST. In the anomaly flows (Fig. 12a), there is a change from weak downslope and offshore flow over Taiwan during the night (most pronounced at 2300 LT) to upslope flow and confluence in the CMR by midday (1400 LT), which coincides with heavy inland rainfall (peak rainfall coverage is again observed at 1700 LT). Similar to UNDIST, rainfall appears to move inland from the west coast throughout the morning (0800–1100 LT) before intensifying substantially over the high terrain as afternoon convection develops (1100–1700 LT; Fig. 7). The flows with their composite mean retained (Fig. 12b) depict interesting relationships between the mei-yu northeasterly flow and diurnal flows in Taiwan. A cyclonic circulation pattern is evident at 2300 LT where downslope and offshore flows drain into the northeasterly flow near southwestern Taiwan. This circulation can also be noted from 0500 to 0800 LT, during which period it shifts eastward in connection with rainfall intensification over southwestern Taiwan (Fig. 12a). This circulation no longer appears once the streamlines around Taiwan transition to onshore and upslope by afternoon.

To assess how persistent this circulation is, as well as the other features in Fig. 12, Fig. 13 displays individual morning (0500 LT) and afternoon (1700 LT) rainfall and surface flow maps from six of the EOP days (31 May–5 June; recall that DIST only includes 31 May–4 June). While the day-to-day variability is indeed pronounced, there is persistence in some of the features. On several mornings, the aforementioned circulation appears with confluence southwest of Taiwan, which resembles a lee vortex in the northeasterly monsoon flow. In the afternoons, in contrast, the flow is more often directed upslope, rainfall is increased over land, and the circulation is usually absent (with the exception of the intense MCV on 5 June). No studies, to our knowledge, have documented a diurnal circulation feature during mei-yu disturbed periods. Thus, the representativeness of these composites needs to be tested by future studies.

Figure 14 presents Taiwan area-averaged diurnal composite vertical profiles of δ, ω, Q_1, and Q_2 for DIST. The mean profiles are qualitatively similar to those

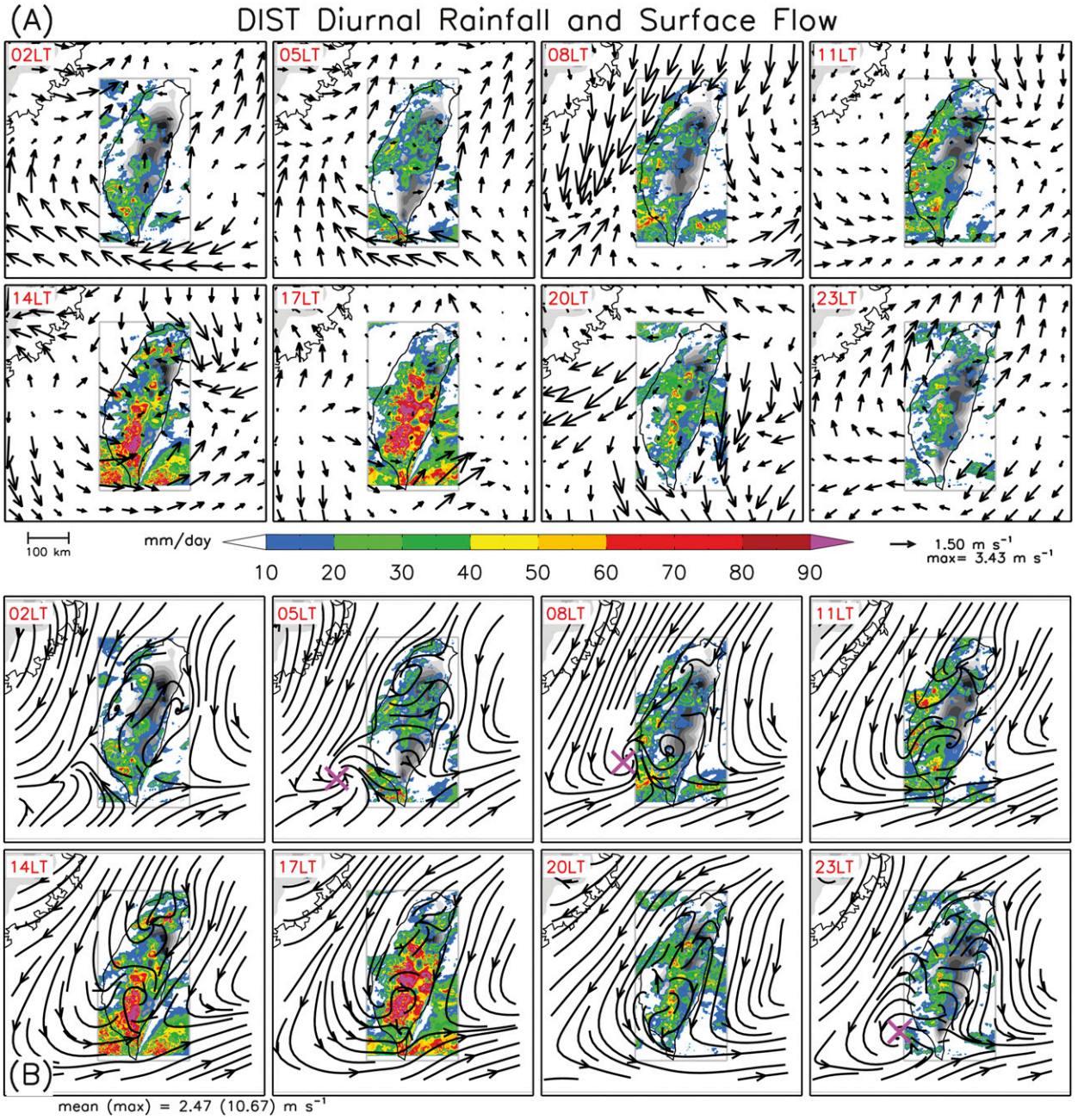

FIG. 12. As in Fig. 9, but for DIST. Note that the rainfall scale is doubled relative to Fig. 9. Also, diurnal flows are provided at 3-hourly frequency during DIST since it coincided with the EOP. The magenta crisscross (×) in (b) marks a circulation center.

during UNDIST (Fig. 10), with stratiform-like structure in vertical motion. As discussed previously, the magnitudes of Q_1 and Q_2 may have small errors in their means associated with unresolved gradients across the CMR and between Taiwan and the surrounding region. The diurnal evolution, however, depicts a sound evolution that is consistent with previous studies (e.g., Johnson and Bresch 1991) and the rainfall maps presented earlier. For instance, note the strong afternoon (1400–1700 LT) deep convection, as indicated by divergence near 200 hPa and rising motion, warming, and drying throughout the column, which coincides with the peak rainfall over the CMR (Figs. 7 and 12). Also note the separation of mid-level Q_1 and Q_2 peaks, indicating the upward transport of eddy heat flux and hence vigorous deep convection (Yanai et al. 1973). An ascending divergence maximum

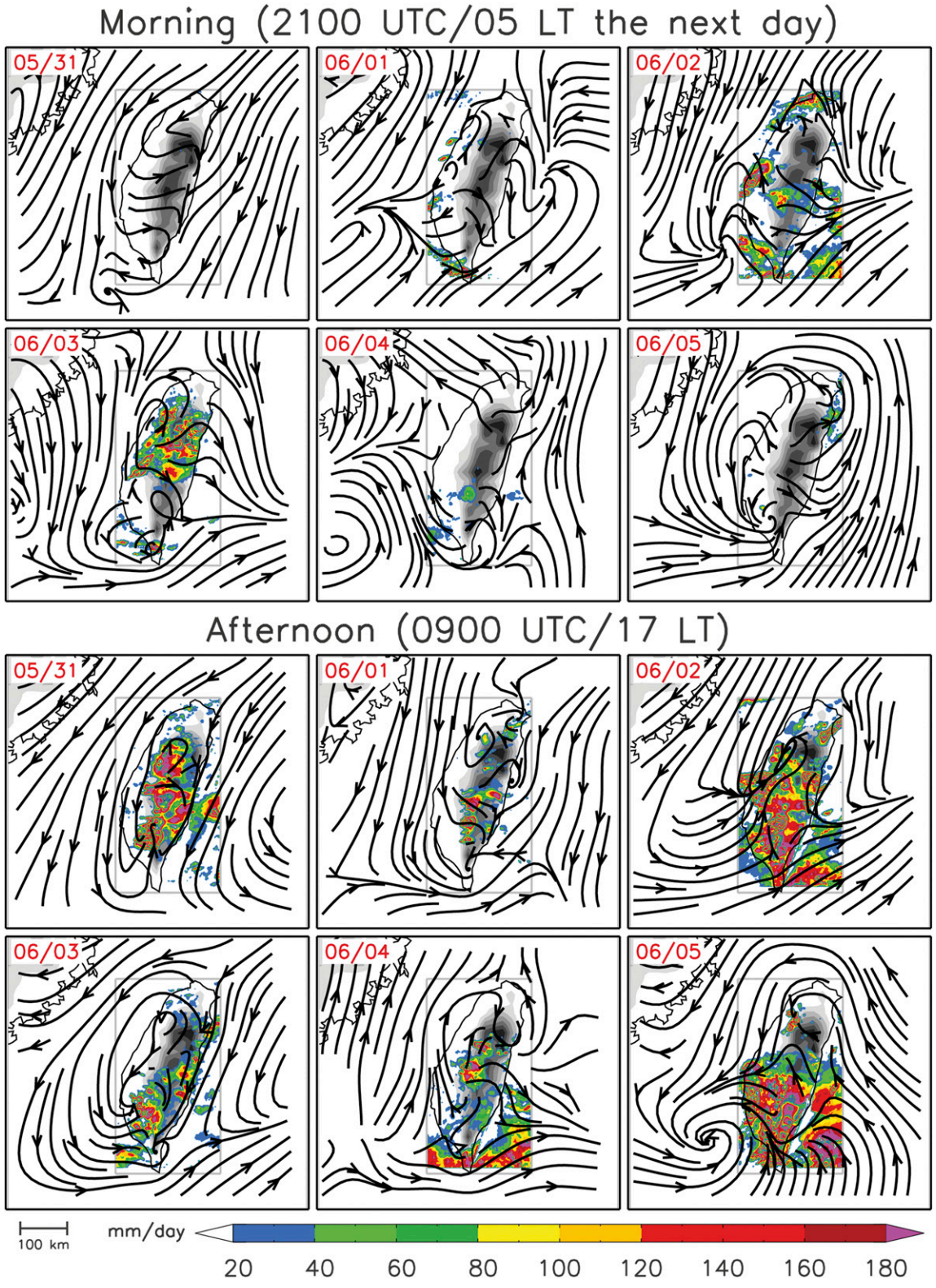

FIG. 13. Surface streamlines and QPESUMS rainfall (mm day^{-1}, shaded) for morning (2100 UTC, 0500 LT the next day) and afternoon (0900 UTC, 1700 LT) on 31 May–5 Jun. Dates are indicated at the top left of each panel, which pertain to UTC time.

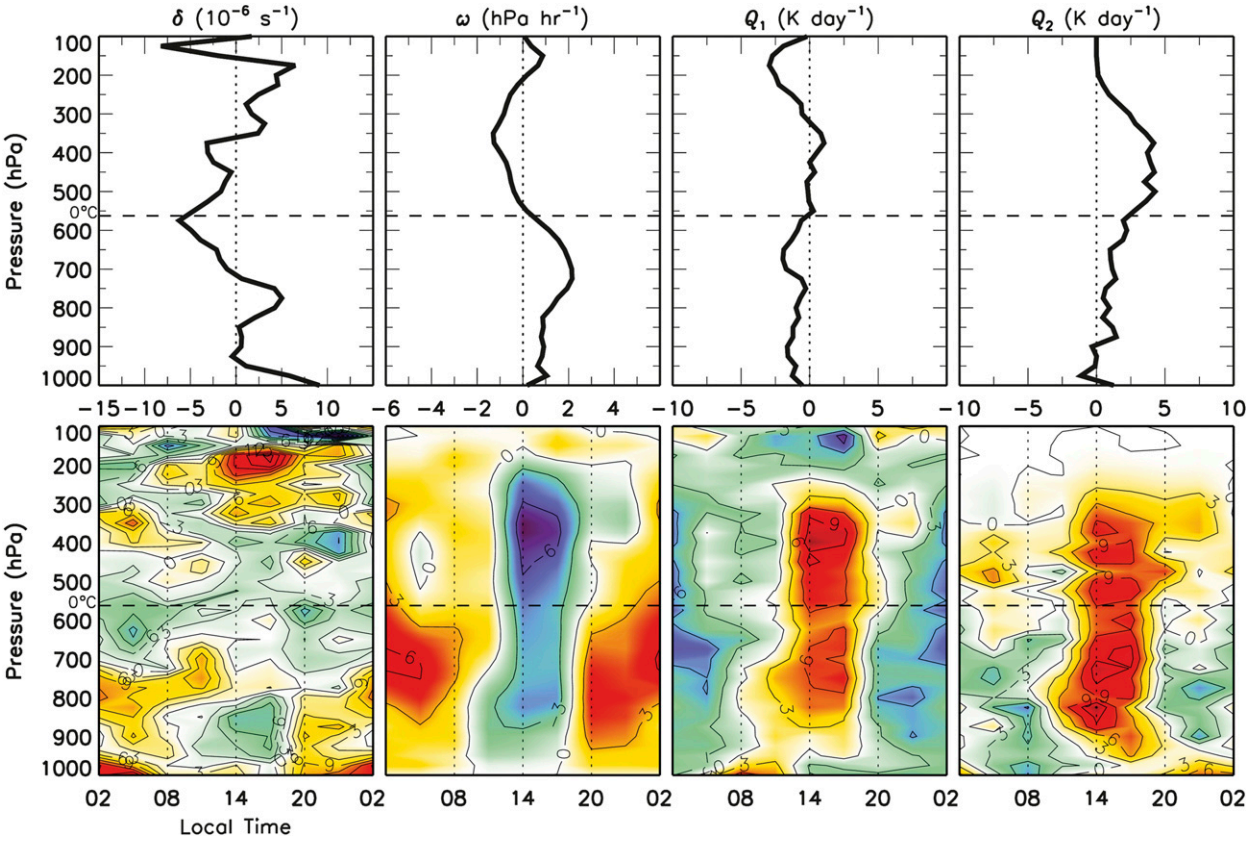

FIG. 14. As in Fig. 10, but for DIST (with 3-hourly sampling).

can be noted (near 800 hPa at 0800 LT) in connection with shallow rising motion and heating preceding deep convection, indicating a deepening shallow cumulus field throughout the morning. By afternoon (2000 LT), a stratiform pattern of elevated rising motion, heating, and drying is evident. This diurnal evolution from shallow cumulus to deep convection to stratiform rain is qualitatively similar to the pattern found during UNDIST (Fig. 10), though the signal of afternoon deep convection is much more pronounced and 3-hourly sampling during the EOP provides improved detail.

5. Discussion

In this study the diurnal cycle during two periods of SoWMEX/TiMREX (2008) has been described: one undisturbed (UNDIST, 22–29 May) and one disturbed (DIST, 31 May–4 June). UNDIST was characterized by relatively uniform southwesterly flow, a dry midtroposphere (Fig. 3), and predominant subsidence (Fig. 4). In association with reduced cloudiness (Fig. 5), there was a strong diurnal cycle in slope flows and rainfall (Fig. 6), with rain peaking in the afternoon over the coastal plains and lower foothills of western Taiwan (Fig. 9). The diurnal cycle in slope flows and rainfall remained important during DIST (Figs. 7, 12, and 14), in spite of strengthened southwesterly flow, a moist troposphere (Fig. 3), and a nearby mei-yu front attended by heavy rainfall (Fig. 11).

A contrasting aspect between DIST and UNDIST is that peak rainfall was shifted upslope during DIST relative to UNDIST (Figs. 8 and 11). The Froude number was larger during DIST in connection with stronger oncoming lower-tropospheric flow, though Fr remained <1 during both periods. Larger Fr is consistent with reduced flow blocking, in which rainfall is expected to be a stronger function of terrain slope (Hughes et al. 2009). In the more disturbed environment during DIST, however, flow–microphysical interactions might have become important with more widespread convection (Jiang 2003; Chen and Lin 2005; Miglietta and Rotunno 2009; Murphy and Businger 2011). Storm microphysical characteristics are discussed next.

Figure 15 provides west–east radar cross sections of reflectivity and hydrometeor identification (HID) for

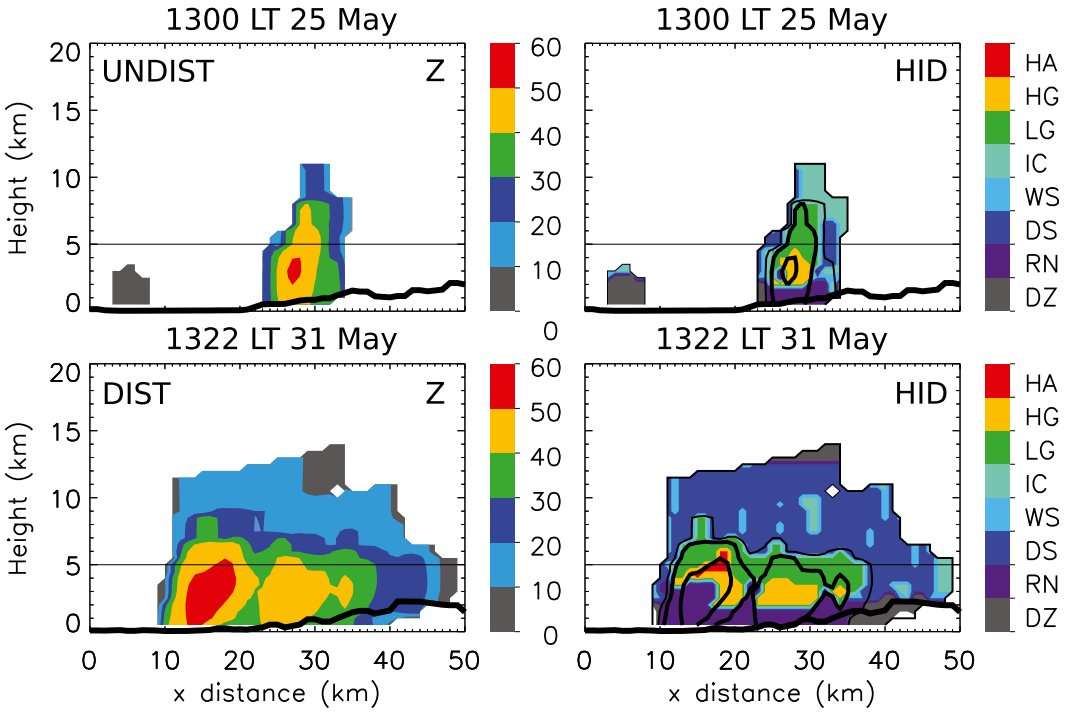

FIG. 15. West-to-east radar cross sections for (top) UNDIST (1300 LT 25 May) and (bottom) DIST (1322 LT 31 May). Cross sections follow the transects shown in Fig. 1 (UNDIST, southernmost transect; DIST, northernmost transect). Abscissa axis is distance from S-Pol radar (km), elevation is shown along the ordinate axis (km), surface elevation is contoured with a thick black line, and the approximate 0°C level is indicated by the thin horizontal line at 5 km. Shown are (left) reflectivity (dBZ, shaded) and (right) HID (shaded), with reflectivity contoured at 0, 30, 40, and 50 dBZ (with 40- and 50-dBZ contours thickened). HID categories are drizzle, DZ; rain, RN; dry snow, DS; wet snow, WS; vertical ice, IC; low-density graupel, LG; high-density graupel, HG; and hail, HA.

two precipitating systems characteristic of UNDIST and DIST (see section 2b for procedures), which are located north of Pingdong (Fig. 1). The most obvious difference between the two precipitating systems in Fig. 15 is in their horizontal extent. While both clearly depict deep convection, with vertically oriented cores of ≥50 dBZ peaking just below the 0°C level (due to the melting of falling graupel), the UNDIST case is more isolated, as was characteristic of diurnal convection during these more undisturbed days (Rowe 2011). The system during DIST (31 May), in contrast, features a more strongly upslope-tilted convective core and a region of elevated graupel of 25–30 km in extent, reflecting a large stratiform region stretching downstream of the system's convective core. The presence of a strongly tilted updraft and large adjoining stratiform region is consistent with the near-saturated environment and strengthened cross-ridge southwesterly flow during DIST (Fig. 3), which aided the lofting of liquid hydrometeors above the 0°C level and, hence, the production of precipitation-sized ice hydrometeors over the higher terrain. Murphy and Businger (2011) documented a similar process in convective storms along the steep slopes of Oahu, Hawaii, during a flooding event in which rainfall was similarly maximized over the highest terrain peaks.

To summarize the key characteristics of the diurnal cycle discussed in this study and the storm-scale processes described above, schematic diagrams of early morning and afternoon flow and rainfall patterns in Taiwan are provided for UNDIST and DIST in Fig. 16. During the early morning hours in UNDIST (DIST), the southwesterly (northeasterly) flow was diverted around Taiwan while the flow within Taiwan was predominately downslope and offshore. Early morning rainfall during both periods was primarily offshore surrounding Taiwan. During the early morning in DIST there was a lee vortex southwest of Taiwan where downslope and offshore flow drained into the postfrontal northeasterly flow. Rainfall was present along the mei-yu front in the northern SCS throughout the day during DIST, with an area of enhanced rainfall just east of the aforementioned early morning circulation [suggesting the possible influence of propagating MCVs in the composite; Lai et al. (2011)]. In the afternoon during both periods, the ambient flow switched to onshore and upslope, as convection developed along the windward slopes. The circulation present

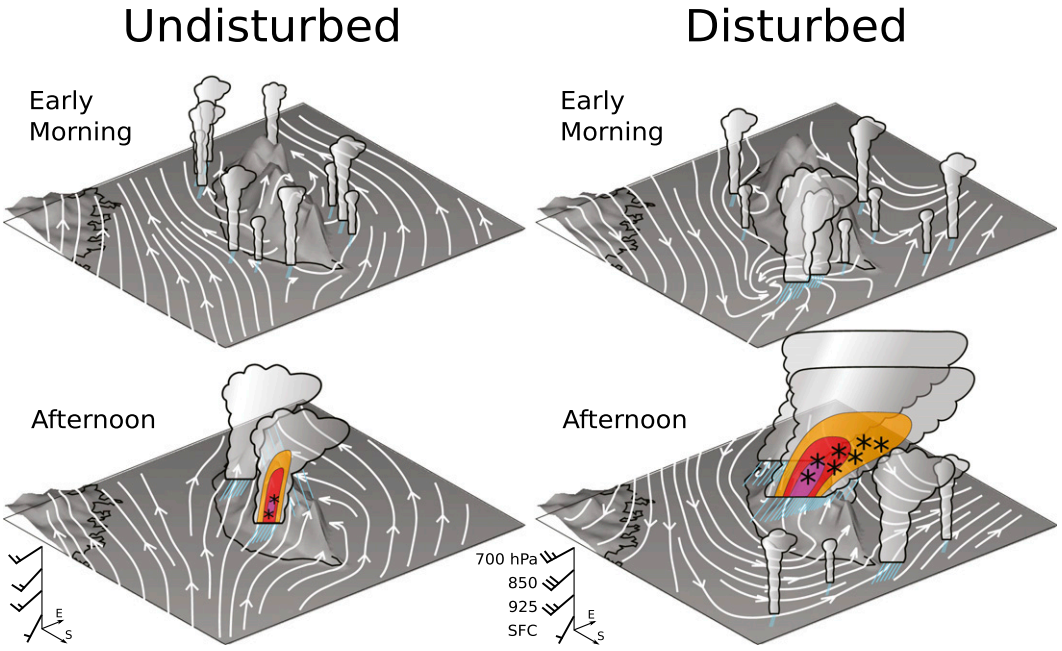

FIG. 16. Schematic depiction of the diurnal cycle looking northeast over Taiwan during the two SoWMEX/TiMREX (2008) periods analyzed in this study. (left) The undisturbed period (22–29 May) was characterized by relatively uniform southwesterly impinging flow, large-scale subsidence, and a dry mid-/upper troposphere over Taiwan. (right) During the disturbed period (31 May–4 Jun), a surface mei-yu front was situated in the northern SCS, the impinging southwesterly flow overriding the front was stronger and moister than UNDIST, and the afternoon rainfall in Taiwan was heavier. Precipitation cores are schematically depicted to exemplify characteristics of afternoon deep convection along the western-coastal plains and windward slopes. Orange, red, and magenta shading patterns indicate radar reflectivity exceeding 30, 40, and 50 dBZ, respectively. Asterisks represent ice hydrometeors. The blue lines indicate rainfall. Surface streamlines are based on 0200 (0500) and 1400 (1700) LT diurnal composites for morning and afternoon during UNDIST (DIST), respectively. Wind profiles are based on UNDIST and DIST mean soundings from Dongsha Island (location indicated in Fig. 8; half and full barbs denote 2.5 and 5 m s^{-1}, respectively). Vertical scale is exaggerated to emphasize terrain, and wind profiles and schematic clouds are not to scale.

during early morning in DIST was absent in the afternoon after the flow switched to onshore and upslope.

Afternoon rainfall was focused along the coastal plains and lower foothills during UNDIST, while rainfall during DIST was maximized in the higher terrain (Fig. 16). Strengthened flow during DIST resulted in more weakly blocked flow, strongly upslope-tilted convective storm cores, and more lofted precipitation-sized ice hydrometeors. These ice hydrometeors were advected over the higher terrain, leading to extensive stratiform regions and the upslope shift in peak rainfall. UNDIST, in contrast, exhibited more isolated convection and more strongly blocked flow, resulting in rainfall peaking farther upstream of the high CMR slopes.

6. Summary and conclusions

The diurnal cycle of mesoscale circulations and rainfall has been described during an undisturbed and a disturbed period of the 2008 Terrain-influenced Monsoon Rainfall Experiment (SoWMEX/TiMREX). This study attempts to improve our understanding of diurnal variability in the presence of steep terrain, and the sensitivity of the diurnal cycle to the strongly varying large-scale environment during Taiwan's mei-yu season. Results for DIST and UNDIST are generally consistent with previous studies of the diurnal cycle in Taiwan (Johnson and Bresch 1991; Chen et al. 1999; Kishtawal and Krishnamurti 2001; Kerns et al. 2010; Lin et al. 2011). However, the enhanced sounding network during the 42-day SoWMEX/TiMREX experiment (13 sites, with 3–6-hourly sampling) allowed us to examine these phenomena with unprecedented detail.

The principal findings of the study are summarized as follows:

- Interpolation of the SoWMEX/TiMREX observational datasets has yielded a detailed gridded analysis,

from which a range of diagnostic analyses and modeling validation efforts can be carried out.

- The diurnal cycle of atmospheric heating and moistening over Taiwan and its vicinity indicates an evolution from shallow cumulus to deep convection (0800–1400 LT) to stratiform rain by evening (2000 LT). This evolution is observed in both disturbed and undisturbed conditions.
- While the amplitude of the diurnal circulations and rainfall activity varies (inversely; Fig. 6) between undisturbed and disturbed conditions, the diurnal evolution in surface flow and rainfall patterns is similar. During the day, offshore rainfall shifts eastward toward the windward slopes of Taiwan as the flow switches to onshore and upslope, and amplifies in the afternoon (1400–1700 LT) along the windward slopes. In the evening, the flow in Taiwan switches to downslope and offshore, and rainfall redevelops in areas of offshore confluence. The coincidence of the switch from upslope to downslope flow with the evening transition to stratiform rain suggests that rainfall evaporation may play a key role in the initiation of the nocturnal katabatic flow, similar to the Big Island of Hawaii (Carbone et al. 1995).
- Although the amplitude of local diurnal circulations is reduced during highly disturbed periods, more favorable characteristics for heavy rainfall make the environment particularly sensitive to these circulations, such that the diurnal variability in rainfall during those periods remains large.
- A circulation pattern resembling a lee vortex is noted during the disturbed period when the ambient flow around Taiwan is northeasterly. This circulation appears near southwestern Taiwan during the night and morning, resembling a lee vortex in the northeasterly flow. The vortex disappears once the flow switches to onshore and upslope. The circulation–rainfall relationship resembles that of an MCV.
- The location of peak rainfall relative to the topography is sensitive to both the nature of the convection and the flow blocking. When the impinging flow is strong (e.g., $15\,m\,s^{-1}$) and the troposphere is conducive to widespread, intense convective storms, greater production of lofted ice hydrometeors and their subsequent advection can lead to a shift in peak rainfall to higher elevations than during undisturbed conditions.

While the results presented for an undisturbed period are consistent with prior studies of the diurnal cycle in Taiwan, few studies have analyzed the diurnal cycle during disturbed summer monsoon conditions. Thus, more years should be compiled to assess the representativeness of the disturbed period results present herein. The sensitivity of the location of peak rainfall relative to topographic barriers to ambient flow characteristics (i.e., tropospheric flow strength and humidity) has very important forecast implications for Taiwan, which is a densely populated country characterized by frequent landslides during the mei-yu season. More detailed analysis of the properties of raining systems during the mei-yu season, such as their microphysical properties and evolution, will enable improved understanding of these sensitivities. The S-Pol radar deployed during SoWMEX/TiMREX provides a great opportunity to do so. Better understanding of the key controls on orographic rainfall properties in this region will improve our ability to predict potentially life-threatening summer monsoon rainfall events.

Acknowledgments. The authors acknowledge Paul Ciesielski for operating the multiquadric interpolation scheme, Dr. Po-Hsiung Lin of NTU for providing data from the NTU experimental forest flux site at Pingdong, and the Central Weather Bureau of Taiwan for providing QPESUMS data. Helpful comments from Paul Ciesielski, Eric Maloney, V. Chandrasekar, Ben Jong-Dao Jou, Steven Fletcher, Hsiao-Wei Lai, Jenny Sun, and Hongli Wang are greatly appreciated. Three anonymous reviewers are also acknowledged for their comments, which substantially improved the study. This research was supported by National Science Foundation Grant AGS-0966758.

APPENDIX

Interpolated Analysis and Taiwan Area Averages

Figure A1 provides UNDIST diurnal composite vertical profiles of Q_1 averaged over Taiwan from three sources: INTERP, INTERP excluding GFS data, and GFS. The most obvious feature in Fig. A1 is the gross overestimation of heating by GFS (relative to INTERP), which would be reflected as overestimated rainfall through the Q_1 budget (Yanai et al. 1973). Furthermore, the diurnal evolution in GFS strongly differs from the other two datasets. The two versions of INTERP are very similar in diurnal evolution, exhibiting daytime shallow-to-deep heating peaks followed by heating over cooling during the evening, indicating stratiform rain.

Figure A2 provides mean and diurnal time–pressure sections of divergence, vertical motion, Q_1, and Q_2 for UNDIST. The only difference from Fig. 10 is that these fields are averaged over western Taiwan instead of the entire island (the dividing line is indicated in Fig. 1). Comparison of Figs. 10 and A2 demonstrates that the

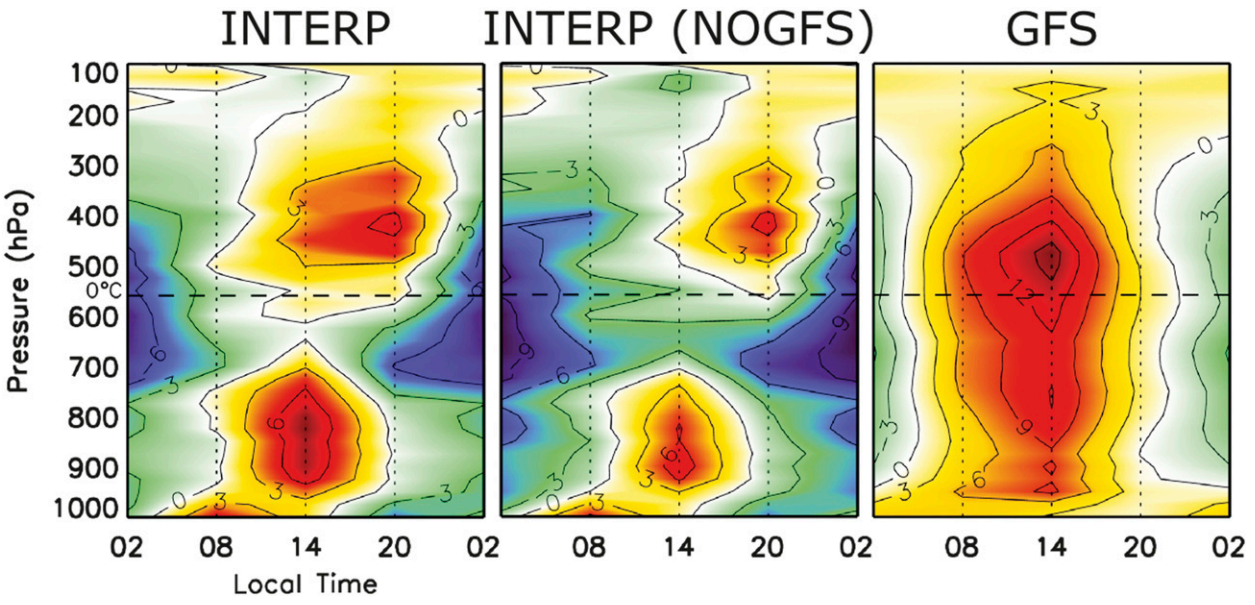

FIG. A1. UNDIST diurnal composite vertical profiles of Q_1 averaged over Taiwan from (left) INTERP, (middle) INTERP but excluding GFS data points, and (right) GFS.

patterns in western Taiwan dominate the full Taiwan averages. This owes to the geographical arrangement in Taiwan, with the main geographic barrier being displaced east of center (Fig. 1). A subtle difference between Figs. 10 and A2 is that the afternoon convection (as seen in rising motion, Q_1, and Q_2) is slightly stronger in Fig. A2, which is consistent with Figs. 8 and 9 showing greater rainfall in western Taiwan.

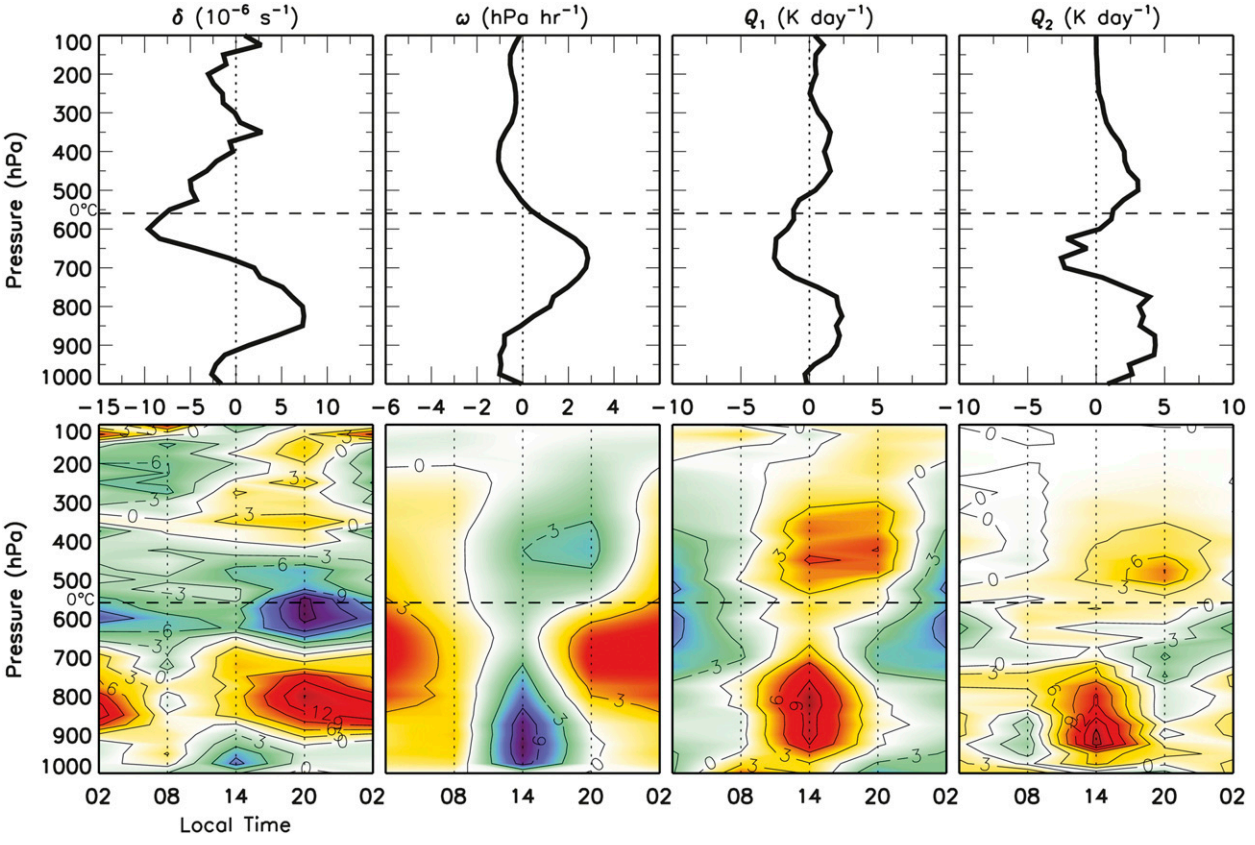

FIG. A2. As in Fig. 10, but fields are averaged over western Taiwan (dividing line indicated in Fig. 1).

REFERENCES

Alpers, W., J.-P. Chen, I.-I. Lin, and C.-C. Lien, 2007: Atmospheric fronts along the east coast of Taiwan studied by ERS synthetic aperture radar images. *J. Atmos. Sci.,* **64,** 922–937.

——, ——, C.-J. Pi, and I.-I. Lin, 2010: On the origin of atmospheric frontal lines off the east coast of Taiwan observed on spaceborne synthetic aperture radar images. *Mon. Wea. Rev.,* **138,** 475–496.

Baines, P. G., 1987: Upstream blocking and airflow over mountains. *Annu. Rev. Fluid Mech.,* **19,** 75–97.

Carbone, R. E., W. A. Cooper, and W.-C. Lee, 1995: Forcing of flow reversal along the windward slopes of Hawaii. *Mon. Wea. Rev.,* **123,** 3466–3480.

Chang, P.-L., P.-F. Lin, B. J.-D. Jou, and J. Zhang, 2009: An application of reflectivity climatology in constructing radar hybrid scans over complex terrain. *J. Atmos. Oceanic Technol.,* **26,** 1315–1327.

Chen, C.-S., W.-C. Chen, and W.-K. Tao, 2004: Characteristics of heavy summer rainfall in southwestern Taiwan in relation to orographic effects. *J. Meteor. Soc. Japan,* **82,** 1521–1543.

Chen, G. T.-J., 1983: Observational aspects of the Mei-Yu phenomenon in subtropical China. *J. Meteor. Soc. Japan,* **61,** 306–312.

——, C.-C. Wang, and S.-W. Chang, 2008: A diagnostic case study of mei-yu frontogenesis and development of wavelike frontal disturbances in the subtropical environment. *Mon. Wea. Rev.,* **136,** 41–61.

Chen, S.-H., and Y.-L. Lin, 2005: Effects of moist Froude number and CAPE on a conditionally unstable flow over a mesoscale mountain ridge. *J. Atmos. Sci.,* **62,** 331–350.

Chen, T.-C., M.-C. Yen, J.-C. Hsieh, and R. W. Arritt, 1999: Diurnal and seasonal variations of the rainfall measured by the Automatic Rainfall and Meteorological Telemetry System in Taiwan. *Bull. Amer. Meteor. Soc.,* **80,** 2299–2312.

Chen, Y.-L., 1993: Some synoptic-scale aspects of the surface fronts over southern China during TAMEX. *Mon. Wea. Rev.,* **121,** 50–64.

Ciesielski, P. E., R. H. Johnson, P. T. Haertel, and J. Wang, 2003: Corrected TOGA COARE sounding humidity data: Impact on diagnosed properties of convection and climate over the warm pool. *J. Climate,* **16,** 2370–2384.

——, and Coauthors, 2010: Quality controlled upper-air sounding dataset for SoWMEX/TiMREX: Development and corrections. *J. Atmos. Oceanic Technol.,* **27,** 1802–1821.

Davis, C. A., and W.-C. Lee, 2012: Mesoscale analysis of heavy rainfall episodes from SoWMEX/TiMREX. *J. Atmos. Sci.,* **69,** 521–537.

Ding, Y. H., and C. L. Chan, 2005: The East Asian summer monsoon: An overview. *Meteor. Atmos. Phys.,* **89,** 117–142.

Durran, D. R., and J. B. Klemp, 1982: On the effects of moisture on the Brunt–Väisälä frequency. *J. Atmos. Sci.,* **39,** 2152–2158.

Houze, R. A., Jr., 1982: Cloud clusters and large-scale vertical motions in the tropics. *J. Meteor. Soc. Japan,* **60,** 396–410.

Huffman, G. J., and Coauthors, 2007: The TRMM Multisatellite Precipitation Analysis (TMPA): Quasi-global, multiyear, combined-sensor precipitation estimates at fine scales. *J. Hydrometeor.,* **8,** 38–55.

Hughes, M., A. Hall, and R. G. Fovell, 2009: Blocking in areas of complex topography, and its influence on rainfall distribution. *J. Atmos. Sci.,* **66,** 508–518.

Jiang, Q., 2003: Moist dynamics and orographic precipitation. *Tellus,* **55A,** 301–316, doi:10.1034/j.1600-0870.2003.00025.x.

Johnson, R. H., 1980: Diagnosis of convective and mesoscale motions during phase III of GATE. *J. Atmos. Sci.,* **37,** 733–753.

——, 1984: Partitioning tropical heat and moisture budgets into cumulus and mesoscale components: Implications for cumulus parameterization. *Mon. Wea. Rev.,* **112,** 1590–1601.

——, and J. F. Bresch, 1991: Diagnosed characteristics of precipitation systems over Taiwan during the May–June 1987 TAMEX. *Mon. Wea. Rev.,* **119,** 2540–2557.

——, and P. E. Ciesielski, 2002: Characteristics of the 1998 summer monsoon onset over the northern South China Sea. *J. Meteor. Soc. Japan,* **80,** 561–578.

——, ——, T. S. L'Ecuyer, and A. J. Newman, 2010: Diurnal cycle of convection during the 2004 North American Monsoon Experiment. *J. Climate,* **23,** 1060–1078.

Jou, B. J.-D., W.-C. Lee, and R. H. Johnson, 2011: An overview of SoWMEX/TiMREX. *The Global Monsoon System: Research and Forecasts,* 2nd ed. C.-P. Chang et al., Eds., World Scientific, 303–318.

Kerns, J. B. W., Y.-L. Chen, and M.-Y. Chang, 2010: The diurnal cycle of winds, rain, and clouds over Taiwan during the mei-yu, summer, and autumn rainfall regimes. *Mon. Wea. Rev.,* **138,** 497–516.

Kishtawal, C. M., and T. N. Krishnamurti, 2001: Diurnal variation of summer rainfall over Taiwan and its detection using TRMM observations. *J. Appl. Meteor.,* **40,** 331–344.

Kummerow, C., and Coauthors, 2000: The status of the Tropical Rainfall Measuring Mission (TRMM) after two years in orbit. *J. Appl. Meteor.,* **39,** 1965–1982.

Kuo, Y.-H., and G. T.-J. Chen, 1990: The Taiwan Area Mesoscale Experiment (TAMEX): An overview. *Bull. Amer. Meteor. Soc.,* **71,** 488–503.

Lai, H.-W., C. A. Davis, and B. J.-D. Jou, 2011: A subtropical oceanic mesoscale convective vortex observed during SoWMEX/TiMREX. *Mon. Wea. Rev.,* **139,** 2367–2385.

Lang, T. J., D. A. Ahijevych, S. W. Nesbitt, R. E. Carbone, S. A. Rutledge, and R. Cifelli, 2007: Radar-observed characteristics of precipitating systems during NAME 2004. *J. Climate,* **20,** 1713–1733.

Li, J., and Y.-L. Chen, 1998: Barrier jets during TAMEX. *Mon. Wea. Rev.,* **126,** 959–971.

Lin, P.-F., P.-L. Chang, B. J.-D. Jou, J. W. Wilson, and R. D. Roberts, 2011: Warm season thunderstorm characteristics under weak synoptic-scale forcing over Taiwan island. *Wea. Forecasting,* **26,** 44–60.

Lin, X., and R. H. Johnson, 1996: Kinematic and thermodynamic characteristics of the flow over the western Pacific warm pool during TOGA COARE. *J. Atmos. Sci.,* **53,** 695–715.

Liu, C., E. J. Zipser, and S. W. Nesbitt, 2007: Global distribution of tropical deep convection: Different perspectives from TRMM infrared and radar data. *J. Climate,* **20,** 489–503.

Liu, H., and V. Chandrasekar, 2000: Classification of hydrometeors based on polarimetric radar measurements: Development of fuzzy logic and neuro-fuzzy systems, and in situ verification. *J. Atmos. Oceanic Technol.,* **17,** 140–164.

Luo, H., and M. Yanai, 1983: The large-scale circulation and heat sources over the Tibetan Plateau and surrounding areas during the early summer of 1979. Part I: Precipitation and kinematic analyses. *Mon. Wea. Rev.,* **111,** 922–944.

Mapes, B. E., P. E. Ciesielski, and R. H. Johnson, 2003: Sampling errors in rawinsonde-array budgets. *J. Atmos. Sci.,* **60,** 2697–2714.

McNab, A. L., and A. K. Betts, 1978: A mesoscale budget study of cumulus convection. *Mon. Wea. Rev.,* **106,** 1317–1331.

Miglietta, M. M., and R. Rotunno, 2009: Numerical simulations of conditionally unstable flows over a mountain ridge. *J. Atmos. Sci.,* **66,** 1865–1885.

Mohr, C. G., L. J. Miller, R. L. Vaughan, and H. W. Frank, 1986: The merger of mesoscale datasets into a common Cartesian format for efficient and systematic analyses. *J. Atmos. Oceanic Technol.,* **3,** 143–161.

Murphy, M. J., and S. Businger, 2011: Orographic influences on an Oahu flood. *Mon. Wea. Rev.,* **139,** 2198–2217.

Nuss, W. A., and D. W. Titley, 1994: Use of multiquadric interpolation for meteorological objective analysis. *Mon. Wea. Rev.,* **122,** 1611–1631.

O'Brien, J. J., 1970: Alternative solutions to the classical vertical velocity problem. *J. Appl. Meteor.,* **9,** 197–203.

Overland, J. E., and N. A. Bond, 1995: Observations and scale analysis of coastal wind jets. *Mon. Wea. Rev.,* **123,** 2934–2941.

Pierrehumbert, R. T., and B. Wyman, 1985: Upstream effects of mesoscale mountains. *J. Atmos. Sci.,* **42,** 977–1003.

Rowe, A. K., 2011: A polarimetric radar analysis of convection observed during NAME and TiMREX. Ph.D. dissertation, Colorado State University, 246 pp. [Available from CSU Libraries, http://lib.colostate.edu/etd.]

——, S. A. Rutledge, and T. J. Lang, 2011: Investigation of microphysical processes occurring in isolated convection during NAME. *Mon. Wea. Rev.,* **139,** 424–443.

——, ——, and ——, 2012: Investigation of microphysical processes occurring in organized convection during NAME. *Mon. Wea. Rev.,* **140,** 2168–2187.

Smolarkiewicz, P. K., R. M. Rasmussen, and T. L. Clark, 1988: On the dynamics of Hawaiian cloud bands: Island forcing. *J. Atmos. Sci.,* **45,** 1872–1905.

Sun, W.-Y., and J.-D. Chern, 1993: Diurnal variation of lee vortices in Taiwan and the surrounding area. *J. Atmos. Sci.,* **50,** 3404–3430.

Tessendorf, S. A., L. J. Miller, K. C. Wiens, and S. A. Rutledge, 2005: The 29 June 2000 supercell observed during STEPS. Part I: Kinematics and microphysics. *J. Atmos. Sci.,* **62,** 4127–4150.

Waliser, D. E., and Coauthors, 2012: The ''year'' of tropical convection (May 2008–April 2010): Climate variability and weather highlights. *Bull. Amer. Meteor. Soc.,* **93,** 1189–1218.

Wang, C.-C., G. T.-J. Chen, T.-C. Chen, and K. Tsuboki, 2005: A numerical study on the effects of Taiwan topography on a convective line during the mei-yu season. *Mon. Wea. Rev.,* **133,** 3217–3242.

Xu, W., E. J. Zipser, Y.-L. Chen, C. Liu, Y.-C. Liou, W.-C. Lee, and B. J.-D. Jou, 2012: An orography-associated extreme rainfall event during TiMREX: Initiation, storm evolution, and maintenance. *Mon. Wea. Rev.,* **140,** 2555–2574.

Yanai, M., S. Esbensen, and J. H. Chu, 1973: Determination of bulk properties of tropical cloud clusters from large-scale heat and moisture budgets. *J. Atmos. Sci.,* **30,** 611–627.

Yeh, H.-C., and Y.-L. Chen, 2002: The role of offshore convergence on coastal rainfall during TAMEX IOP 3. *Mon. Wea. Rev.,* **130,** 2709–2730.

Yu, C.-K., and B. J.-D. Jou, 2005: Radar observations of the diurnally forced offshore convective lines along the southeastern coast of Taiwan. *Mon. Wea. Rev.,* **133,** 1613–1636.

——, and C.-Y. Lin, 2008: Statistical location and timing of the convective lines off the mountainous coast of southeastern Taiwan from long-term radar observations. *Mon. Wea. Rev.,* **136,** 5077–5094.

——, and Y.-H. Hsieh, 2009: Formation of the convective lines off the mountainous coast of southeastern Taiwan: A case study of 3 January 2004. *Mon. Wea. Rev.,* **137,** 3072–3091.